

1 **Cloud vertical structure over a tropical station obtained using long-term**
2 **high resolution Radiosonde measurements**

3 Nelli Narendra Reddy, Madineni Venkat Ratnam*, Ghouse Basha and Varaha Ravikiran
4 National Atmospheric Research Laboratory, Department of Space, Gadanki-517112, India.

5 *vratnam@narl.gov.in

6 **Abstract**

7 Cloud vertical structure, including top and base altitudes, thickness of cloud layers,
8 and the vertical distribution of multi-layer clouds affects the large-scale atmosphere
9 circulation by altering gradients in the total diabatic heating/cooling and latent heat release. In
10 this study, long-term (11 years) observations of high vertical resolution radiosondes are used
11 to obtain the cloud vertical structure over a tropical station, Gadanki (13.5° N, 79.2° E), India.
12 The detected cloud layers are verified with independent observations using cloud particle
13 sensor (CPS) sonde launched from the same station. High-level clouds account for 69.05%,
14 58.49%, 55.5%, and 58.6% of all clouds during pre-monsoon, monsoon, post-monsoon, and
15 winter seasons, respectively. The average cloud base (cloud top) altitude for low-level,
16 middle-level, high-level and deep convective clouds are 1.74 km (3.16 km), 3.59 km (5.55
17 km), 8.79 km (10.49 km), and 1.22 km (11.45 km), respectively. Single-layer, two-layer, and
18 three-layer clouds account for 40.80%, 30.71%, and 19.68% of all cloud configurations,
19 respectively. Multi-layer clouds occurred more frequently during the monsoon with 34.58%.
20 Maximum cloud top altitude and the cloud thickness occurred during monsoon season for
21 single-layer clouds and the uppermost layer of multiple layer cloud configurations. In multi-
22 layer cloud configurations, diurnal variations in the thickness of upper layer clouds are larger
23 than those of lower layer clouds. Heating/cooling in the troposphere and lower stratosphere
24 due to these cloud layers is also investigated and found peak cooling (peak warming) below
25 (above) the Cold Point Tropopause (CPT) altitude. The magnitude of cooling (warming)

26 increases from single-layer to four or more-layer cloud occurrence. Further, the vertical
27 structure of clouds is also studied with respect to the arrival date of Indian summer monsoon
28 over Gadanki.

29 **Keywords:** Cloud vertical structure, Single-layer clouds, Multi-layer clouds, Cloud base, top
30 and thickness

31

32 **1. Introduction**

33 Clouds are vital in driving the climate system as they play important role in radiation
34 budget, general circulation and hydrological cycle (Ramanathan et al., 1989; Rossow and
35 Lacis, 1990; Wielicki et al., 1995; Li et al., 1995; Stephens, 2005; Yangetal., 2010;
36 Huang,2013). By interacting with both shortwave and long-wave radiation, clouds play
37 crucial role in the radiative budget at the surface, within and at the top of the atmosphere (Li
38 et al., 2011; Ravi Kiran et al., 2015; George et al., 2018). Clouds and the general circulation
39 of Earth's atmosphere are linked in an intimate feedback loop. Clouds result from the water
40 vapor transports and cooling by atmospheric motions. The forcing for the atmospheric
41 circulation is significantly modified by vertical and horizontal gradients in the radiative and
42 latent heat fluxes induced by the clouds (Chahine et al., 2006 and Li et al., 2005). The
43 complexity of the processes involved, the vast amount of information needed, including
44 vertical and spatial distribution, and the uncertainty associated with the available data, all add
45 difficulties to determine how clouds contribute to climate change (e.g., Heintzenberg and
46 Charlson, 2009). In particular, knowledge about cloud type is very important, because the
47 overall impact of clouds on the Earth's energy budget is difficult to estimate, as it involves
48 two opposite effects depending on cloud type (Naud et al., 2003). Low, highly reflective
49 clouds tend to cool the surface, whereas high, semi-transparent clouds tend to warm it,
50 because they let much of the shortwave radiation through but are opaque to the longwave

51 radiation. Whereas deep convective clouds (DCCs) neither warm nor cool the surface,
52 because their cloud greenhouse and albedo forcing's nearly balance. However, DCCs
53 produce fast vertical transport, redistributing water vapor and chemical constituents and
54 influence the thermal structure of the Upper Troposphere and Lower Stratosphere (UTLS)
55 (Biondi et al., 2012).

56 Changes in the cloud vertical structure (locations of cloud top and base, number and
57 thickness of cloud layers) affect the atmospheric circulations by modifying the distribution of
58 radiative and latent heating rates within the atmosphere (e.g., Slingo and Slingo, 1988;
59 Randall et al., 1989; Slingo and Slingo, 1991; Wang and Rossow, 1998; Li et al., 2005 and
60 Chahine et al., 2006; Cesana and Chepfer, 2012; Rossow and Zhang, 2010; Rossow et al.,
61 2005; Wang et al., 2014b). The effects of cloud vertical structure (CVS) on atmospheric
62 circulation have been described using atmospheric models by many authors. Crewell et al.
63 (2004) underlined the importance of clouds in multiple scattering and absorption of sunlight,
64 processes that have a significant impact on the diabatic heating in the atmosphere. The
65 vertical gradients in the cloud distribution were somewhat more important to the circulation
66 strength than horizontal gradients (Rind and Rossow, 1984). These complex phenomena are
67 not yet fully understood and are subject to large uncertainties. In fact, the assumed or
68 computed vertical structure of cloud occurrence in general circulation models (GCMs) is one
69 of the main reasons why different models predict a wide range of future climates. For
70 example, most GCMs underestimate the cloud cover, while only a few overestimate it (Xi et
71 al., 2010). Therefore, to improve the understanding of cloud-related processes, and then to
72 increase the predictive capabilities of large-scale models (including global circulation
73 models), better and more accurate observations of CVS is needed. The present work is a
74 contribution towards addressing this need.

75 Ground-based instruments (e.g. Warren et al., 1988; Hahn et al., 2001), active sensor
76 satellites (e.g. Stephens et al., 2008; Winker et al., 2007) and upper air measurements from
77 radiosondes (Wang et al., 2000) are usually applied to observe and describe the CVS.
78 Ground-based instruments such as lidar, cloud radar and ceilometers provide cloud
79 measurements with continuous temporal coverage; Lidars and ceilometers are very efficient
80 at detecting clouds and can locate the bottom of cloud layer precisely, but cannot usually
81 detect the cloud top, due to attenuation of the beam within the cloud. The vertically pointing
82 cloud radar is able to detect the cloud top, although signal artifacts can cause difficulties
83 during precipitation (Nowak et al., 2008). On the other hand, passive sensor satellite data,
84 such as from ISCCP (the International Satellite Cloud Climatology Project) and MODIS (the
85 Moderate Resolution Imaging Spectroradiometer), do exist limitations. For example, the thin
86 clouds are indistinguishable from aerosols in ISCCP when optical thickness is less than 0.3–
87 0.5) (Rossow and Garder, 1993); Both ISCCP and MODIS underestimate low-level clouds
88 and overestimate middle-level cloud (Li et al., 2006; Naud and Chen, 2010). Hence,
89 conventional passive-sensor satellite measurement, largely miss the comprehensive
90 information on the vertical distribution of cloud layers. The precipitation radar and TRMM
91 Microwave Imager on-board the Tropical Rainfall Measuring Mission (TRMM) satellite are
92 helpless in observing small-size particles despite of its capability of penetrating rainy cloud
93 and obtaining the internal three-dimensional information, and only larger rainfall particles
94 can be observed due to limitations of its working broadband. On the other hand, active
95 sensors such as the Cloud Profiling Radar (CPR) on CloudSat and the Cloud-Aerosol Lidar
96 with Orthogonal Polarization (CALIOP) aboard CALIPSO (Cloud Aerosol Lidar and Infrared
97 Pathfinder Satellite Observation) satellites are achieving notable results by including a
98 vertical dimension to traditional satellite images. CPR is a 94 GHz nadir-looking radar which
99 is able to penetrate the optically thick clouds, while CALIOP is able to detect tenuous cloud

100 layer that are below the detection threshold of radar. In other words, it has the ability to detect
101 shallow clouds. Therefore, accurate location of cloud top and complete vertical structure
102 information of cloud can be obtained by the combined use of CPR and CALIOP, because of
103 their unique complementary skills. Previous researches have shown that CloudSat/CALIPSO
104 data are credible compared with ISCCP and ground observation data (Sassen and Wang,
105 2008; Naud and Chen, 2010; Kim et al., 2011; Noh et al., 2011; Jiang et al., 2011). However,
106 because the repeat time of these polar orbiting satellites for any particular location is very
107 large, the time resolution of such observations is low (L'Ecuyer and Jiang, 2010; Qian et al.,
108 2012). Both ground-based and space-based measurements have the problem of overlapping
109 cloud layers that hide each other.

110 For completeness here we listed other techniques which have been developed for
111 detecting cloud top heights from passive sensors. The CO₂-slicing method uses CO₂
112 differential absorption in the thermal infrared spectral range (Rossow and Schiffer, 1991;
113 King et al., 1992; Platnick et al., 2003). Ultraviolet radiances can also be used as rotational
114 Raman scattering causes depletion or filling of solar Fraunhofer lines in the UV spectrum,
115 depending on the Rayleigh scattering above the cloud (Joiner and Bhartia, 1995; de Beek et
116 al., 2001). Similarly, the polarization of reflected light, at visible shorter wavelength, due to
117 Rayleigh scattering carries information on cloud top height (Goloub et al., 1994; Knibbe et
118 al., 2000). Finally, cloud top height can also be retrieved by applying geometrical methods to
119 stereo observations (Moroney et al., 2002; Seiz et al., 2007; Wu et al., 2009). Global
120 Navigation Satellite System (GNSS) Radio Occultation (RO) profiles were used to detect the
121 convective cloud top heights (Biondi et al., 2013). Recently, Biondi et al. (2017) used GNSS
122 RO profiles to detect the top altitude of volcanic clouds and analyzed their impact on thermal
123 structure of UTLS. Multi-angle and bi-spectral measurements in the O₂ A-band were used to
124 derive the cloud top altitude and cloud geometrical thickness (Merlin et al., 2016 and

125 references therein). However, this method is restricted to homogeneous plane-parallel clouds.
126 For heterogeneous clouds or when aerosols lay above the clouds the spectra of reflected
127 sunlight in the O₂ A-band will get modified.

128 An indirect way to perform estimations of CVS is by using atmospheric thermodynamic
129 profiles as measured by radiosondes. Radiosondes can penetrate atmospheric (and cloud)
130 layers to provide in situ data. The profiles of temperature, relative humidity and pressure
131 measured by radiosondes provide information about the CVS by identifying saturated levels
132 in the atmosphere (Zhang et al., 2010). In fact, radiosonde measurements were probably the
133 best measurements for obtaining the CVS from the ground (Wang et al., 2000; Eresmaa et al.,
134 2006; Zhang et al., 2010). Very recently, George et al. (2018) provided CVS over India
135 during depression (D) and non-depression (ND) events during South West monsoon season
136 (July 2016) using one month of campaign data. However, detailed CVS in all the seasons
137 including diurnal variation over Indian region is not made so far to the best of our knowledge.

138 Our main objective is to examine the temperature structure of UTLS region during the
139 occurrence of single-layer and multi-layer clouds over Gadanki location (13.5° N, 79.2° E). In
140 the first, we focus to report the CVS using long-term (11 years) high vertical resolution
141 radiosondes observations. The paper is organized as follows: data and methodology are
142 described in section 2. In section 3, background weather conditions during the period of
143 analysis are described. Results and discussion are given in section 4. Finally, the summary
144 and major conclusion drawn from the present study is provided in section 5.

145 **2. Data and Methodology**

146 **2.1. Data**

147 In this study, long-term (11 years) observations of high vertical resolution radiosonde
148 (Vaisälä RS-80, RS-92; Meisei RS-01GII, RS-6G, RS-11G, IMS-100) data is used to analyze
149 CVS over a tropical station, Gadanki. There is no significant change in the accuracies of the

150 meteorological parameters from these different radiosonde makes. Most of these radiosondes
151 were launched around 1730 Local Time, LT (LT=UT+0530 h). In general we will not release
152 the balloon during moderate to heavy rain conditions. However, we have done visual
153 inspection of each radiosonde profile. RH profiles which show continuous saturation with
154 height were discarded. Figure 1 shows the monthly percentage of radiosonde data available
155 during Apr. 2006 to May 2017. Total 3313 launches were made, out of which 98.9% and
156 86.6% reached altitudes greater than 12.5 km and 20 km, respectively. The data which have
157 balloon burst altitude less than 12.5 km (1.1%) are discarded. Also, we have put condition
158 that the number of profiles in a month should be more than seven to represent that month.
159 After applying these two conditions the total number of profiles came to 3251. In addition, to
160 study the diurnal variations in CVS over Gadanki, we made use of radiosonde observations
161 taken from Tropical Tropopause Dynamics (TTD) campaigns (Venkat Ratnam et al., 2014b)
162 conducted during Climate and Weather of Sun Earth Systems (CAWSES) India Phase II
163 program (Pallamraju et al., 2014). During these campaigns, the radiosondes were launched
164 every three hourly for continuous three days in each month during Dec. 2010 to Mar. 2014
165 except in Dec. 2012, Jan., Feb., Apr., 2013.

166 **2.2. Methodology**

167 There are several methods available in the literature to determine the CVS from the
168 profiles of radiosonde data (Poore et al., 1995; Wang and Rossow, 1995; Chernykh and
169 Eskridge, 1996; Minnis et al., 2005; Zhang et al., 2010). Poore et al. (1995) estimated the
170 cloud base and cloud top using temperature-dependent dew-point depression thresholds. First,
171 the dew-point depression must be calculated at every radiosonde level. According to Poore et
172 al. (1995), a given atmospheric level has a cloud if $\Delta T_d < 1.7^\circ\text{C}$ at $T > 0^\circ\text{C}$, $\Delta T_d < 3.4^\circ\text{C}$ at 0
173 $> T > -20^\circ\text{C}$, $\Delta T_d < 5.2^\circ\text{C}$ at $T < -20^\circ\text{C}$.

174 Wang and Rossow (1995) used the temperature, pressure and RH profiles and computed RH
175 with respect to ice instead of liquid water for levels with temperatures lower than 0 °C. To
176 this new RH profile they have applied two RH thresholds (min RH = 84% and max RH =
177 87%). In addition, if RH at the base (top) of the moist layer is lower than 84%, a RH jump
178 exceeding 3% must exist from the underlying (above) level. According to the Chernykh and
179 Eskridge (1996) method, the necessary condition for the existence of clouds in a given
180 atmospheric level is that the second derivatives with respect to height (z) of temperature and
181 RH to be positive and negative, respectively ie., $T''(z) \geq 0$ and $RH''(z) \leq 0$. Minnis et al.
182 (2005) provided an empirical parameterization that calculates the probability of occurrence of
183 a cloud layer using RH and air temperature from radiosondes. First, RH values must be
184 converted to RH with respect to ice when temperature is less than -20 °C; on the other hand,
185 the profile has to be interpolated every 25 hPa up to the height of 100 hPa. An expression to
186 estimate the cloud probability (P_{cld}) as a function of temperature and RH is then applied; in
187 this formula, where RH is given the maximum influence as it is the most important factor in
188 cloud formation. Finally, a cloud layer is set wherever $P_{cld} \geq 67\%$. The Zhang et al. (2010)
189 method is an improvement on the Wang and Rossow (1995) method. Instead of a single RH
190 threshold, Zhang et al. (2010) applied altitude-dependent thresholds without the requirement
191 of the 3% RH jump at the cloud base and top.

192 Costa-Suros et al. (2014) compared the CVS derived from these five methods described
193 above by using 193 radiosonde profiles acquired at the Atmospheric Radiation Measurement
194 (ARM) Southern Great Plains site during all seasons of the year 2009. The performance of
195 the five methods has been assessed by comparing with Active Remote Sensing of Clouds
196 (ARSCL) data taken as a reference. Costa-Suros et al. (2014) concluded that three of the
197 methods (Poore et al., 1995; Wang and Rossow, 1995; and Zhang et al., 2010) perform
198 reasonably well, giving perfect agreements for 50% of the cases and approximate agreements

199 for 30% of the cases. The other methods gave poorer results (lower perfect and/or
200 approximate agreement, and higher false positive, false negative or not coincident
201 detections). Among the three methods, Zhang et al. (2010) method is the most recent version
202 of the treatment initially proposed in Poore et al. (1995) and Wang and Rossow (1995), and
203 provides good enough results (a perfect agreement of 53.9% and an approximate agreement
204 of 29.5%). Thus, the algorithm of Zhang et al. (2010) is used for detecting cloud layers in our
205 analysis and we provide details of Zhang et al. (2010) algorithm.

206 Cloud layers are associated with high RH values above some threshold as the radiosonde
207 penetrates through them. Cloud detection algorithm of Zhang et al. (2010) employs three
208 height-resolving RH thresholds to determine cloud layers: minimum and maximum RH
209 thresholds in cloud layers (min-RH and max-RH), and minimum RH thresholds within the
210 distance of two contiguous layers (inter-RH). The height-resolving thresholds of max-RH,
211 min-RH, and inter-RH values are specified in Table 1. The algorithm begins by converting
212 RH with respect to liquid water to RH with respect to ice at temperatures below 0° C (see
213 example in Figure 2). The accuracy of RH measurement is less than 5% up to the altitude
214 12.5 km and hence the RH profile is examined from the surface to the 12.5 km (~ 200 hPa)
215 altitude to find cloud layers in seven steps: (1) the base of the lowest moist layer is
216 determined as the level when RH exceeds the min-RH corresponding to this level; (2) above
217 the base of the moist layer, contiguous levels with RH over the corresponding min-RH are
218 treated as the same layer; (3) the top of the moist layer is identified when RH decreases to
219 that below the corresponding min-RH or RH is over the corresponding min-RH but the top of
220 the profile is reached; (4) moist layers with bases lower than 500 m AGL (Above Ground
221 Level) and thickness less than 400 m are discarded; (5) the moist layer is classified as a cloud
222 layer if the maximum RH within this layer is greater than the corresponding max-RH at the
223 base of this moist layer; (6) two contiguous layers are considered as a one-layer cloud if the

224 distance between these two layers is less than 300 m or the minimum RH within this distance
225 is more than the maximum inter-RH value within this distance; and (7) clouds are discarded
226 if their thicknesses are less than 100 m.

227 At measurement location, we have Boundary Layer Lidar and Mie Lidar. When there is
228 occurrence of multi-layer configuration, BLL does not give accurate cloud base altitude for
229 higher layers. Whereas, Mie LIDAR gives the vertical structure of the cirrus clouds (usually
230 occur at higher altitude). In the present study, CVS is examined only up to 12.5 km altitude as
231 the accuracy in RH measurements is poor at higher altitudes. Also, Mie LIDAR is operated
232 mostly during cloud free conditions (only during cirrus cloud or clear sky conditions).
233 Further, the timings of Radiosonde and LIDAR measurements are different. Hence, we did
234 not do inter comparison study with ground based LIDAR observations. On the other hand,
235 CLOUDSAT/CALIPSO overpasses over experiment location are around 02 LT and 14 LT.
236 Whereas regular radiosonde launches are around 1730 LT. Hence, we did not do inter
237 comparison study between regular radiosonde and CLOUDSAT/CALIPSO measurements.
238 However, we have three hourly radiosonde observations for continuous three days in every
239 month during TTD campaigns. Unfortunately, we did not get collocated (space and time)
240 measurements from CLOUDSAT/CALIPSO and Radiosonde during these campaigns.

241 Before proceeding further, it is desired to verify the identified layers of clouds are correct
242 or not with independent observations. For that we have launched Cloud Particle Sensor (CPS)
243 sonde (Fujiwara et al., 2016) at Gadanki, which provides profile of cloud number
244 concentration. Results from a flight of RS-11G radiosonde and Cloud Particle Sensor (CPS)
245 Sonde on the same balloon launched at 02 LT on 04 Aug. 2017 at Gadanki, India is shown in
246 Figure 2. Sudden increase in the cloud number concentration within the detected cloud layers
247 indicates the cloud layer boundaries detected in the present study are accurate.

248 The drawback of using the radiosonde data for detecting the CVS at a given location is
249 the radiosonde horizontal displacement, due to the drift produced by the wind. However,
250 irrespective of the season, the maximum horizontal drift of radiosonde when it reaches the
251 12.5 km altitude is always less than 20 km (Venkat Ratnam et al., 2014a). One may expect
252 different background features within this 20 km particularly the localised convection that may
253 influence the CVS. In order to assess this aspect, we used outgoing longwave radiation
254 (OLR) as a proxy for tropical convection. Figure 3(a-d) describes the seasonal mean
255 distribution of OLR (from KALPANA-1 satellite) around Gadanki location obtained during
256 pre-monsoon, monsoon, post-monsoon and, winter seasons averaged during 2006 – 2017. It
257 can be noted that irrespective of the season, homogeneous cloudiness prevailed for more than
258 50 km radius around Gadanki location. Hence the CVS detected from the radiosonde can be
259 treated as representative of Gadanki location.

260 Methodology described in section 2.2 to detect CVS is applied on high vertical resolution
261 radiosonde data acquired during Apr. 2006 to May 2017 from Gadanki, as well as special
262 radiosondes launches during TTD campaigns from Oct. 2010 to Apr. 2014. Results are
263 presented in Section 4. Before going further, it is desirable to examine the background
264 meteorological conditions prevailing over Gadanki during different seasons.

265 **3. Background meteorological conditions**

266 National Atmospheric Research Laboratory (NARL) at Gadanki is located about 120 km
267 northwest of Chennai (Madras) on the east coast of the southern Indian peninsula. This
268 station is surrounded by hills with a maximum altitude of 350–400 m above the station, and
269 the station is at an altitude of 375 m a.m.s.l. (hereinafter all altitudes are mentioned above
270 mean sea level only). The local topography is complex with a number of small hillocks
271 around and a high hill of ~1 km about 30 km from the balloon launching site in the northeast
272 direction. The detailed topography of Gadanki is shown in Basha and Ratnam (2009).

273 Gadanki receives 53% of the annual rainfall during the southwest monsoon (Jun. to Sep.) and
274 33% of the annual rainfall during the northeast monsoon (Oct. to Dec.) (Rao et al., 2008a).
275 The rainfall during the southwest monsoon occurs predominantly during the evening to
276 midnight period. About 66% of total rainfall is convective in nature, while the remaining rain
277 is widespread stratiform in character (Rao et al., 2008a).

278 Background meteorological conditions prevailing over the observational site are briefly
279 described based on the radiosonde data collected during Apr. 2006 to May 2017. The seasons
280 are classified as winter (December-January- February), pre-monsoon (March-April-May),
281 monsoon (June-July-August-September), post-monsoon (October-November). The
282 climatological monthly mean contours of the temperature anomalies, relative humidity, zonal
283 and meridional winds are shown in Figure 4(a-d), respectively. From surface to 1 km
284 altitude, temperature anomalies show seasonal variability with warmer temperatures during
285 pre-monsoon months and relatively cooler temperatures during winter season (Figure 4a).
286 Temperature anomalies do not show significant variations seasonally from 1 km altitude to
287 the middle troposphere, but shows variations in the lower stratosphere. There exist significant
288 seasonal variations in the RH (Figure 4b). During winter, RH is small (40 – 50%) from
289 surface to ~ 3 km altitude and is almost negligible above. However, during the other seasons,
290 particularly in the peak monsoon months (Jul. and Aug.), large RH values (60–70%) are
291 noticed up to 10 km altitude.

292 During winter, easterlies exist up to 4–6 km altitude and westerlies above (Figure 4c).
293 There seem to be weak easterlies above the altitude of 14 km during the pre-monsoon. During
294 the monsoon season low level westerlies exist below 7–8 km and easterlies above. The
295 Tropical Easterly Jet (TEJ) is prevalent over this region in the SW monsoon season, with
296 peak velocity sometimes reaching more than 40 ms^{-1} (Roja Raman et al., 2009). There exist
297 large vertical shears during monsoon in the zonal wind. Easterlies exist up to 20 km altitude

298 during post-monsoon season. In general, meridional velocities are very small and are
299 northerlies up to 8 km and southerlies above in all the seasons, except during monsoon
300 (Figure 4d). During the winter and monsoon, relatively stronger southerlies and northerlies
301 prevailed, respectively, between 12 to 15 km altitudes. A clear annual oscillation can be
302 noticed in both zonal and meridional velocities. Similar variations are also observed by the
303 MST radar located at the same site in between 4 and 20 km (Ratnam et al., 2008; Basha and
304 Ratnam, 2009; Debashis Nath et al., 2009). Monthly mean OLR around Gadanki at 1730 LT
305 is shown in Figure 4e. Low values of OLR ($< 220 \text{ W m}^{-2}$) around Gadanki location indicate
306 that the occurrence of very deep convection during the monsoon season, consistent with the
307 occurrence of high RH values up to 10 km altitude during monsoon season (Figure 4b).

308 **4. Results**

309 By adopting the methodology described in section 2.2 we have detected a total of 4309
310 Cloud layers from 3251 radiosonde launches at Gadanki location during the period of data
311 analysis. For each season, cloud layers during Apr. 2006 – May 2017 are averaged to obtain
312 the composite picture of CVS. Seasonal variability in cloud layers is discussed in section 4.2.

313 **4.1. Diurnal variation of single-layer and multi-layer clouds**

314 There are studies on the diurnal variation of cloud layers outside the Indian region. For
315 example, over Porto Santo Island during the Atlantic Stratocumulus Transition Experiment
316 (ASTEX) by Wang et al. (1999), over San Nicolas Island during First ISCCP Regional
317 Experiment (FIRE) by Blaskovic et al. (1990), Over Shouxian (32.56° N , 116.78° E) location
318 by Zhang et al. (2010). As per authors knowledge there are no studies on diurnal variability
319 of cloud layers over Indian region. For the first time, over Indian land region, the diurnal
320 variability of cloud layers are studied by using radiosonde observations taken from TTD
321 campaigns. Figure 5(a-d) describes the diurnal variations of single-layer and multi-layer
322 clouds during pre-monsoon, monsoon, post-monsoon, and winter seasons over Gadanki

323 region. As mentioned in section 2.1, from Dec. 2010 to Mar. 2014, we have launched
324 radiosondes every three hourly for continuous three days in every month except during Dec.
325 2012, Jan., Feb., Apr., 2013. The total number of profiles taken during pre-monsoon,
326 monsoon, post-monsoon, and winter seasons are 160, 254, 101, and 199, respectively.
327 Among these the number of cloudy profiles are 93 in pre-monsoon, 241 in monsoon, 63 in
328 post-monsoon, and 96 in winter seasons.

329 From the Figure 5(a-d), for four seasons, diurnal variations of cloud occurrence show a
330 maximum between 23 to 05 LT and a minimum at 14 LT, except during monsoon season.
331 During monsoon season, a minimum in cloud occurrence occurred at 11 LT. Using Infrared
332 Brightness temperature data over Indian region Gambheer and Bhat (2001), Zuidema (2003),
333 Reddy and Rao (2018) observed the maximum frequency of occurrence of clouds during late
334 night early morning hours. Percentage occurrence of one-layer and multi-layer clouds shows
335 noticeable diurnal variations in all seasons except in monsoon season. Maximum percentage
336 occurrence in one-layer clouds is at 08 LT in pre-monsoon season and it is at 17 LT during
337 post-monsoon and winter seasons. For all the seasons, the maximum percentage occurrence
338 in multi-layer clouds is between 20 to 05 LT. Figure 6(a-d) describes the mean vertical
339 locations (base and top) and cloud thicknesses of one-layer clouds during pre-monsoon,
340 monsoon, post-monsoon, and winter seasons, respectively. During monsoon season, the
341 maximum in cloud top altitude is at 05 LT and minimum is at 14 LT (Figure 6(b)). In general,
342 cloud base of one-layer cloud occur at higher altitude between 11 – 14 LT and it occur
343 relatively low altitudes between 20 – 08 LT. Except during post-monsoon season, the single-
344 layer clouds are high-level clouds with base is greater than 5 km most of the times. During
345 post-monsoon season, the single-layer clouds are low-level at 05 LT (cloud-base altitude of
346 1.4 km) and middle level-clouds between 14 – 02 LT (Figure 6c). During pre-monsoon and
347 monsoon seasons, thickness of single-layer clouds reaching a maximum at 23 LT and a

348 minimum at 14 LT (Figure 6(a-b)). The minimum in one-layer cloud thickness at 14 LT is
349 due to the increase of cloud base altitude and simultaneous decrease of cloud top altitude.
350 There is not much variability in thickness of one-layer clouds during post-monsoon and
351 winter seasons (Figure 6(c-d)). Figure 7(a-d) and Figure S1(a-d) are same as Figure 6(a-d)
352 but for two-layer and three-layer clouds. Similar to one-layer cloud, the cloud base of bottom-
353 layer of two-layer clouds show maximum between 11 – 14 LT and minimum between 20 –
354 08 LT. Thickness of top layer and bottom layer of two-layer clouds reaching a minimum
355 value between 11 – 14 LT. Upper layer of two-layer clouds show a maximum in thickness at
356 23 LT and minimum at 11 LT during monsoon season (Figure 7(b)).

357 The cloud maintenance and development are strongly modulated by diabatic processes,
358 namely solar heating and longwave (LW) radiative cooling (Zhang et al., 2010). Near
359 noontime (11 - 14 LT), solar heating is so strong that (1) evaporation of cloud drops may
360 occur and (2) atmospheric stability may increase thus suppressing cloud development. So
361 near noontime, the vertical development of single-layer clouds and the vertical development
362 of the uppermost layer of multiple layers of cloud are suppressed due to solar heating. This
363 effect is predominant during monsoon season for one-layer and two-layer clouds (Figures
364 6(b) and 7(b)), during pre-monsoon and post-monsoon seasons for three-layer clouds (Figures
365 S1a and S1c). However, for lower layers of cloud in a multiple-layer cloud configuration,
366 solar heating is greatly reduced because of the absorption and scattering processes of the
367 upper layers of cloud. In general maximum in surface temperature occurs around 15:20 LT
368 (Reddy and Rao, 2018). The ground surface is warmer than any cloud layer so through the
369 exchange of LW radiation, the cloud base gains more energy. This facilitates cloud
370 development and leads to a maximum in cloud altitude and thickness between 14 – 17 LT
371 (Figures 7a, 7b, 7d and S1a). This effect is predominant during winter season for two layer
372 clouds (Figure 7d) and during pre-monsoon season for three-layer clouds (Figure S1a). As the

373 sun sets, LW radiative cooling starts to dominate over shortwave (SW) radiative warming.
374 Cloud top temperatures begin to lower, which increases atmospheric instability and fuels the
375 development of single-layer clouds and the uppermost layer of cloud in multiple-layer cloud
376 configurations. At sunset, solar heating diminishes and LW cooling strengthens, which may
377 explain why there is a peak between 20 – 23 LT in the thickness of one-layer clouds and the
378 uppermost layer of two-layer cloud. This effect is clearly observed in the monsoon season
379 (Figures 6b, 7b, S1b). We conclude that diurnal variability in base, top and thickness for
380 single-layer, two-layer and, three-layer clouds are significant. Hence there can be a bias in
381 cloud vertical structure when we are studying the composite over a season by using polar
382 satellites.

383 Next section, we show the seasonal variability in cloud layers using long-term (11 years)
384 observations of high vertical resolution radiosonde over Gadanki. Note that most of these
385 radiosondes were launched around 1730 LT hence there will be bias in the results due to
386 diurnal variability of cloud layers which we have discussed above. Hence the results related
387 to seasonal variability of cloud layers are only representative of 1730 LT.

388 **4.2. Seasonal variability in the cloud layers**

389 Figure 8(a-c) describes the percentage occurrence of base, top and thickness of cloud
390 layers observed during different seasons over Gadanki. The cloud base altitude shows a
391 bimodal distribution in all seasons except during pre-monsoon season (Figure 8a). During
392 pre-monsoon season, the peak of cloud base altitude distribution is observed at ~6.2 km
393 (~7.5%). During other three seasons (monsoon, post-monsoon and winter), the first peak in
394 cloud base altitude is observed between 2 and 3 km altitude region and the second peak is
395 observed at ~6.2 km. Using CLOUDSAT observations over the Indian monsoon region, Das
396 et al. (2017) also reported that the cloud base altitude over Indian monsoon region shows a

397 bimodal distribution. However, the first peak in cloud base altitude is observed at ~14 km
398 while the second maximum is at 2 km.

399 The cloud top altitude increases above 12 km altitude and have a maximum at 12.5 km in
400 all seasons (Figure 8b). Note that we restrict maximum altitude as 12.5 km due to limitation
401 in providing reliable water vapor above that altitude from normal radiosondes. At lower
402 altitudes, during the monsoon season the peak in cloud top altitude is at 2.9 km and it
403 increases to 3.3 km during the post-monsoon season. However we have also checked the
404 cloud vertical structure till 18 km. There is no significant difference in the cloud base and
405 cloud top altitude distribution (See Figure S2). Das et al. (2017) reported that there are two
406 peaks in the cloud top altitude; one at ~17 km and other is at ~3 km. The peaks in cloud base
407 and cloud top at higher altitudes as observed by Das et al. (2017) could be due to the
408 occurrence of cirrus clouds.

409 The cloud base altitude values are subtracted from the cloud top altitude for each cloud
410 layer to extract the cloud thickness. Figure 8(c) describes the percentage occurrence of the
411 cloud thickness observed during different seasons. The occurrence of thicker clouds
412 decreases exponentially. The cloud thickness has a maximum below 500 m for all seasons,
413 which constituted about 34.7%, 26.5%, 31.2% and 36.6% of the total observed cloud layers
414 during pre-monsoon, monsoon, post-monsoon and winter seasons, respectively. In general,
415 for all seasons, more than 65% of clouds layers have cloud thickness < 2 km.

416 Different cloud types occurring at different height regions have a spectrum of effects on
417 the radiation budget (Behrangi et al., 2012). Therefore, the clouds have been classified into
418 four groups based on the cloud base altitude and their thickness (Lazarus et al., 2000 and
419 Zhang et al., 2010): (1) low-level clouds with bases lower than 2 km and thickness less than 6
420 km; (2) middle-level clouds with bases ranging from 2 to 5 km; (3) high-level clouds with
421 bases greater than 5 km; and (4) deep convective cloud (hereafter called DCC) with base less

422 than 2 km and thicknesses greater than 6 km. These four types of clouds account for 11.97%,
423 26.71%, 59.36% and 1.95% of all cloudy cases, respectively. Figure 9(a-d) describe the mean
424 vertical locations (base and top), cloud thicknesses and percentage occurrence of low-,
425 middle-, high-level clouds, and DCC observed during different seasons. At Gadanki location,
426 there is a distinct persistence of the high-level clouds over all the seasons. The occurrence of
427 the high-level clouds is 69.05%, 58.49%, 55.5%, 58.6% during the pre-monsoon, monsoon,
428 post-monsoon, and winter seasons, respectively (Figure 9c). In general, after the dissipation
429 of deep convective clouds they spread large anvils and remain persist as high level clouds for
430 longer duration. These high level clouds could be due to in-situ generated Convective
431 Systems or else propagated from the surrounding Oceans. Zuidema (2003) reported that the
432 deep convective systems generated over central and west Bay of Bengal (BoB) advect toward
433 the inland region of southern peninsular India and dissipates. In general, the high level clouds
434 follow background winds at those levels. Especially during monsoon season, due to the
435 strong westerly winds in the upper levels, high level clouds which are originated from MCS
436 over BoB advect into the Indian land region and contribute to the high level cloud
437 occurrence. Hence the outflow caused by the deep convective systems could be responsible
438 for the higher percentage occurrence of high-level clouds. The low-level (middle-level)
439 clouds contribute about 3.74%, 10.45%, 16.27%, and 20.89% (27.04%, 29.35%, 24.28%, and
440 18.67%) of all cloudy cases during the pre-monsoon, monsoon, post-monsoon, and winter
441 seasons, respectively (Figure 9a-b).

442 Thicknesses of low-, middle-, high-level clouds have minimum values during winter
443 season and maximum values in monsoon season (Figure 9a-c). Whereas DCC have minimum
444 thickness in winter and maximum in pre-monsoon season (Figure 9d). The average cloud
445 base (cloud top) altitudes for low-, middle-, high-level clouds and deep convective clouds are
446 1.74 km (3.16 km), 3.59 km (5.55 km), 8.79 km (10.49 km), and 1.22 km (11.45 km),

447 respectively. Over Indian summer monsoon region, Das et al. (2017) reported that the
448 percentage occurrence of high-level clouds is more than the other three cloud types. Over
449 Shouxian (32.56° N, 116.78° E) location, Zhang et al. (2010) reported that the percentage
450 occurrence of low-, middle-, high-level clouds and deep convective clouds is 20.1%, 19.3%,
451 59.5%, and 1.1%, respectively.

452 **4.2.1. Single-layer and Multi-layer clouds**

453 By interacting with both shortwave and longwave radiation, clouds play crucial role in the
454 radiative budget at the surface, within and at the top of the atmosphere. Over the tropics, the
455 zonal mean net cloud radiative effect differences between multi-layer clouds and single-layer
456 clouds were positive and dominated by the shortwave cloud radiative effect differences (Li et
457 al., 2011). This is because, the multi-layer clouds reflect less sunlight to the top of the
458 atmosphere and transmit more to the surface and within the atmosphere than the single-layer
459 clouds as a whole. As a result, multi-layer clouds warm the earth-atmosphere system when
460 compared to single-layer clouds (Li et al., 2011). In this study, we studied the occurrence of
461 single-layer and multi-layer clouds obtained during different seasons at Gadanki location.
462 The percentage occurrence of single-layer, two-layer, three-layer and four- or more- layer
463 clouds during pre-monsoon, monsoon, post-monsoon and winter seasons are shown in Figure
464 10(a-d). Single-layer, two-layer and three-layer clouds account for 40.80%, 30.71%, and
465 19.68% of all cloud configurations, respectively. Even though the low frequency of
466 occurrence of one-layer clouds over Gadanki, they exhibit pronounced seasonal variation in
467 magnitude with very low frequency during pre-monsoon season. This may be due to the
468 strong warm and dry atmospheric conditions from surface to boundary layer top (Figure 4a
469 and 4b). Percentage occurrence of single-layer (multi-layer) clouds during pre-monsoon,
470 monsoon, post-monsoon and winter seasons are 7.7%, 14.2%, 8.48% and 10.42% (7.93%,
471 34.58%, 10.83% and 5.86%), respectively. There is a significant occurrence of multi-layer

472 clouds during monsoon season than other seasons indicating that the development of multi-
473 layer clouds is favorable under warm and moist atmospheric conditions (Figures 4a and 4b).
474 Among the different cloud layers, the two-layer clouds have maximum percentage occurrence
475 (16.6%) during monsoon season (Figure 10b). Luo et al. (2009) reported the occurrence of
476 multi-layer clouds over the Indian region during the summer season and attributed it to the
477 complex cloud structure associated with the monsoon system. Zhang et al. (2010) reported
478 that multi-layer cloud occurrence frequency is relatively higher during summer months (Jun.,
479 Jul. and Aug.) than autumn months (Sep., Oct. and Nov.) over Shouxian. Recently, Using the
480 four years of combined observations of Cloudsat and CALIPSO, Subrahmanyam and Kumar
481 (2017) reported the maximum frequency of occurrence of two-layer clouds over Indian sub-
482 continent during Jun. Jul. and Aug months. This they attributed to the presence of Indian
483 summer monsoon circulation over this region, which is dominated by the formation of
484 various kinds of clouds such as cumulus, stratocumulus, cirrus etc.,. Very recently, George et
485 al. (2018) reported CVS using the radiosonde launches during depression (D) and non-
486 depression (ND) events in South West monsoon season using one month of field campaign
487 data over Kanpur, India.

488 Figure 11(a-c) describe the mean vertical locations (base and top) and cloud thicknesses
489 of single-layer, two-layer and three-layer clouds during different seasons. Except during
490 winter season, single-layer clouds are thicker than the layers forming multi-layer clouds.
491 Also, upper layer clouds are thicker than lower layer clouds in multi-layer clouds. This could
492 be due to the exchange of longwave radiation between cloud base of upper layer and cloud
493 top of lower layer. As a result, the strong reduction in longwave radiation cooling at the top
494 of the lower layer of cloud in the presence of upper layers of cloud (Zhang et al., 2010; Wang
495 et al., 1999; Chen and Cotton, 1987).

496 Irrespective of the season, single-layer clouds are high-level clouds i.e cloud base is >
497 5 km (Figure 11a). Maximum cloud top altitude and the cloud thickness occurred during
498 monsoon season for single-layer clouds (Figure 11a) and the uppermost layer of multi-layer
499 cloud configurations (Figure 11b-c). This is consistent with the low OLR values ($< 220 \text{ W}$
500 m^{-2}) observed during monsoon season (Figure 11d). Except during pre-monsoon season,
501 cloud base, cloud top and cloud thickness values of lower layer of multi-layer clouds are
502 same during monsoon, post-monsoon and winter seasons. Whereas during pre-monsoon
503 season, cloud base and cloud top of lower layer of multi-layer clouds occurred at relatively
504 higher altitudes (Figure 11b-c). Similarly, there are no significant variations in cloud
505 thickness in middle layer of three-layer clouds between the seasons. However, cloud base and
506 cloud top of middle layer of three-layer clouds during pre-monsoon season occurred
507 relatively at higher altitudes than the other three seasons (Figure 11c). Table 2 describes the
508 mean base, top and thicknesses of cloud layers of single-layer, two-layer and three-layer
509 clouds. In the two-layer clouds, the thickness of the upper level cloud layer is about the same
510 as those of single-layer clouds. In the three-layer clouds, the base and top heights of the
511 lowest layer of cloud are similar to those of the lowest layer of cloud in two-layer clouds.

512 **4.3. Variability in CVS with respect to SW monsoon arrival over Gadanki**

513 CVS play an important role in the summer monsoon because they can significantly affect
514 the atmospheric heat balance through latent heating caused by water phase changes and
515 through scattering of radiation. In this section we discuss the variability in different clouds
516 with respect to the date of arrival of southwest (SW) monsoon over Gadanki. SW monsoon
517 onset occurs over Kerala coast (south west coast of India) during the last week of the May or
518 first week of June. In general, the climatological mean monsoon onset over Kerala (MOK) is
519 on 1 June with ± 7 days. It is to be noted that the climatology onset date is obtained from IMD

520 long term onset dates and arrival date over Gadanki is picked up manually from the yearly
521 onset date lines over India map given by IMD.

522 Figure 12 shows the composite (2006 – 2016) percentage occurrence of clear sky and
523 cloud days (Figure 12a), low-level, middle-level, high-level and deep convective clouds
524 (Figure 12b), and one-, two-, three- and four or more- layer clouds (Figure 12c) with respect
525 to monsoon arrival date. Figures 13(a-c) describe the mean vertical locations (base and top)
526 and cloud thicknesses of single-layer, two-layer clouds with respect to monsoon arrival date.
527 Day zero in Figures 12(a-b) and Figures 13(a-b) indicates the date of monsoon arrival over
528 Gadanki location. The percentages occurrences of clear sky conditions prior to the monsoon
529 arrival over Gadanki location decreases and reduce to zero on the date of monsoon arrival
530 (Figure 12a). This indicates the estimated dates of monsoon arrival over Gadanki location are
531 correct. From day four onwards the cloudiness start increases and peaks on day 18 (Figure
532 12a). The percentage occurrence of middle level clouds decreases till 5 days prior to the
533 monsoon arrival (Figure 12b). Subsequently middle level clouds percentage increases and
534 does not show significant variability later to the monsoon arrival. There are no deep
535 convective clouds prior and during the monsoon arrival over Gadanki location (Figure 12b).
536 They occurred on day 3, 9, 10, 17 and 20. During and later to the arrival of the monsoon, the
537 percentage occurrence of multilayer clouds is always greater than the single layer clouds
538 except day three and four (Figure 12c). Day zero it is noted that single layer clouds are high
539 level clouds and they are thicker with thickness ~ 6.7 km (Figure 13a). In two layer clouds
540 the bottom layer is middle layer cloud and top layer is high level cloud (Figure 13b). The
541 bottom layer is thicker than the top layer. During deep convective clouds and middle level,
542 single layer clouds prevailed. The thickness of single layer clouds show large variability with
543 thickness ranging from 300 m to 5 km during the first week later to the arrival of the
544 monsoon. In the second week, the thickness ranges from 2 km to 5 km (Figure 13a). Later to

545 the arrival of the monsoon, thickness of bottom layer in two layer cloud is relatively higher
546 than the top layer (Figure 13b). Thicker single layer clouds and bottom layer of two layer
547 clouds later to the monsoon arrival over Gadanki is due to the increase of tropospheric water
548 vapor.

549 **5. Summary**

550 Cloud vertical structure (CVS) is studied for the first time over India by using long-term
551 high vertical resolution radiosonde measurements at Gadanki location obtained during Apr.
552 2006 to May 2017. In order to obtain diurnal variation in CVS, we have used 3 hourly
553 launched radiosondes for 3 days in each month during Dec. 2010 to Mar. 2014. CVS is
554 obtained following Zhang et al. (2010) where it relay on height-resolved relative humidity
555 thresholds. After obtaining the cloud layers they are segregated to low, middle and high level
556 clouds depending upon their altitude of occurrence. Detected layers are verified using
557 independent measurements from cloud particle sensor (CPS) sonde launched from same
558 location. Very good match between these two independent measurements is noticed.

559 First, the diurnal variations in CVS over Gadanki is studied using radiosonde
560 observations taken from TTD campaigns conducted during CAWSES India Phase II program.
561 During pre-monsoon and monsoon seasons, thickness of single-layer clouds reaches a
562 maximum at 23 LT and a minimum at 14 LT. Upper layer of two-layer clouds show a
563 maximum in thickness at 23 LT and minimum at 11 LT during monsoon season. Radiosonde
564 measurements around 1730 LT were used to study the seasonal variability in CVS. After
565 ascertaining the cloud layers they are segregated into different season to obtain the season
566 variation of CVS. High-level clouds account for 69.05%, 58.49%, 55.5%, and 58.6% of cloud
567 layers identified during pre-monsoon, monsoon, post-monsoon, and winter seasons,
568 respectively, indicating high cloud layers being most prevalent at Gadanki location. Single-
569 layer, two-layer, and three-layer clouds account for 40.80%, 30.71%, and 19.68% of all cloud

570 configurations, respectively. Multi-layer clouds occurred more frequently during the
571 monsoon with 34.58%. Maximum cloud top altitude and the cloud thickness occurred during
572 monsoon season for single-layer clouds and the uppermost layer of multi-layer cloud
573 configurations.

574 Further, we have discussed the variability in different clouds with respect to the date of
575 arrival of southwest (SW) monsoon over Gadanki location. Prior, during and later to the SW
576 monsoon arrival over Gadanki location, high level clouds occurrence is more than the other
577 cloud types. Whereas the middle level cloud occurrence decreases till 5 days prior to the
578 monsoon arrival and increases subsequently. There are no deep convective clouds prior and
579 during the monsoon arrival over Gadanki location. The thickness of single layer clouds shows
580 large variability during the first week later to the arrival of the monsoon. But it increases
581 significantly between 8 – 11 days later to the monsoon arrival. Later to the arrival of the
582 monsoon, thickness of bottom layer in two layer cloud is relatively higher than the top layer.
583 Thicker single layer clouds and bottom layer of two layer clouds later to the monsoon arrival
584 over Gadanki is due to the increase of tropospheric water vapor.

585 These cloud layers are expected to affect significantly to the background temperature
586 in the troposphere and lower stratosphere. The composite (2006-2016) temperature profiles
587 during clear sky, one-layer, two-layer, three-layer and four or more-layer cloud occurrences
588 are shown in Figure 14. The temperature differences between the cloudy (single-, two-, three-
589 , four or more- layer) and clear sky conditions are shown with dash lines in Figure 14. The
590 striking result here is that occurrence of peak cooling (peak warming) below (above) the Cold
591 Point Tropopause (CPT) altitude. The magnitude of cooling (warming) increases from single-
592 layer to four or more-layer cloud occurrence. The peak cooling and warming during four or
593 more-layer cloud occurrence are 0.9 K (at 15.7 km) and 3.6 K (at 18.1 K). Both single-layer
594 and multi-layer clouds shows warming between 5 km and 14.5 km altitude region. The peak

595 warming of 0.8 K at 9.5 km for single-layer cloud, and 1.3 K at 10.2 K for multi-layer clouds
596 are observed and these altitudes are close to the cloud top altitude of single layer cloud and
597 top layer of multi-layer clouds (Table 2). The detailed study on the impact of single-layer and
598 multi-layer clouds on UTLS dynamics and thermodynamics structure will be investigated in
599 our subsequent article including their radiative forcing.

600 **Acknowledgements**

601 We are grateful to the staffs of National Atmospheric Research Laboratory (NARL),
602 Gadanki, who are involved in GPS radiosonde launching. Data used in the present study can
603 be obtained on request. We thank associate editor and three anonymous reviewers for
604 providing constructive comments/suggestions which made us to improve the manuscript
605 content further.

606 **References**

- 607 Basha, G., Ratnam, M.V.: Moisture variability over Indian monsoon regions observed using
608 high resolution radiosonde measurements. *Atmos. Res.* 132–133, 35–45.
609 doi:10.1016/j.atmosres.2013.04.004, 2013.
- 610 Basha, G., Ratnam, M.V.: Identification of atmospheric boundary layer height over a tropical
611 station using high-resolution radiosonde refractivity profiles: Comparison with GPS radio
612 occultation measurements. *J. Geophys. Res. Atmos.* 114, D16101.
613 doi:10.1029/2008JD011692, 2009.
- 614 Behrangi, A., Kubar, T., Lambrigtsen, B.: Phenomenological Description of Tropical Clouds
615 Using CloudSat Cloud Classification. *Mon. Weather Rev.* 140, 3235–3249.
616 doi:10.1175/MWR-D-11-00247.1, 2012.
- 617 Biondi, R., Randel, W. J., Ho, S.-P., Neubert, T. and Syndergaard, S.: Thermal structure of
618 intense convective clouds derived from GPS radio occultations, *Atmos. Chem. Phys.*, 12(12),
619 5309–5318, doi:10.5194/acp-12-5309-2012, 2012.

620 Biondi, R., Ho, S.-P., Randel, W.J., Neubert, T., Syndergaard, S.: Tropical cyclone cloud-top
621 height and vertical temperature structure detection using GPS radio occultation
622 measurements. *J. Geophys. Res. Atmos.* 118, 5247–5259. doi:10.1002/jgrd.50448, 2013.

623 Biondi, R., Steiner, A. K., Kirchengast, G., Brenot, H. and Rieckh, T.: Supporting the
624 detection and monitoring of volcanic clouds: A promising new application of Global
625 Navigation Satellite System radio occultation, *Adv. Sp. Res.*, 60(12), 2707–2722, doi:
626 10.1016/j.asr.2017.06.039, 2017.

627 Blaskovic, M., Davies, R., Snider, J.B.: Diurnal Variation of Marine Stratocumulus over San
628 Nicolas Island during July 1987. *Mon. Weather Rev.* 119, 1469–1478. doi:10.1175/1520-
629 0493(1991)119<1469:DVOMSO>2.0.CO;2, 1990.

630 Cesana, G., Chepfer, H.: How well do climate models simulate cloud vertical structure? A
631 comparison between CALIPSO-GOCCP satellite observations and CMIP5 models. *Geophys.*
632 *Res. Lett.* 39, n/a-n/a. doi:10.1029/2012GL053153, 2012.

633 Chahine, M.T., Pagano, T.S., Aumann, H.H., Atlas, R., Barnet, C., Blaisdell, J., Chen, L.,
634 Divakarla, M., Fetzer, E.J., Goldberg, M., Gautier, C., Granger, S., Hannon, S., Irion, F.W.,
635 Kakar, R., Kalnay, E., Lambrigtsen, B.H., Lee, S.-Y., Le Marshall, J., McMillan, W.W.,
636 McMillin, L., Olsen, E.T., Revercomb, H., Rosenkranz, P., Smith, W.L., Staelin, D., Strow,
637 L.L., Susskind, J., Tobin, D., Wolf, W., Zhou, L.: AIRS: Improving Weather Forecasting and
638 Providing New Data on Greenhouse Gases. *Bull. Am. Meteorol. Soc.* 87, 911–926.
639 doi:10.1175/BAMS-87-7-911, 2006.

640 Chen, C., Cotton, W.R.: The Physics of the Marine Stratocumulus-Capped Mixed Layer. *J.*
641 *Atmos. Sci.* 44, 2951–2977. doi:10.1175/1520-0469(1987)044<2951:TPOTMS>2.0.CO;2,
642 1987.

643 Chernykh, I. V, Eskridge, R.E.: Determination of Cloud Amount and Level from Radiosonde

644 Soundings. *J. Appl. Meteorol.* 35, 1362–1369. doi:10.1175/1520-
645 0450(1996)035<1362:DOCAAL>2.0.CO;2, 1996.

646 Costa-Surós, M., Calbó, J., González, J.A., Long, C.N.: Comparing the cloud vertical
647 structure derived from several methods based on radiosonde profiles and ground-based
648 remote sensing measurements. *Atmos. Meas. Tech.* 7, 2757–2773. doi:10.5194/amt-7-2757-
649 2014, 2014.

650 Crewell, S., Bloemink, H., Feijt, A., García, S.G., Jolivet, D., Krasnov, O.A., Van Lammeren,
651 A., Löhnert, U., Van Meijgaard, E., Meywerk, J., Quante, M., Pfeilsticker, K., Schmidt, S.,
652 Scholl, T., Simmer, C., Schröder, M., Trautmann, T., Venema, V., Wendisch, M., Willén, U.:
653 THE BALTEX BRIDGE CAMPAIGN: An Integrated Approach for a Better Understanding
654 of Clouds. *Bull. Am. Meteorol. Soc.* 85, 1565–1584. doi:10.1175/BAMS-85-10-1565, 2004.

655 Das, S.K., Golhait, R.B., Uma, K.N.: Clouds vertical properties over the Northern
656 Hemisphere monsoon regions from CloudSat-CALIPSO measurements. *Atmos. Res.* 183,
657 73–83. doi:https://doi.org/10.1016/j.atmosres.2016.08.011, 2017.

658 de Beek, R., Vountas, M., Rozanov, V. V., Richter, a., and Burrows, J. P.: The ring effect in
659 the cloudy atmosphere, *Geophys. Res. Lett.*, 28, 721–724, doi:10.1029/2000GL012240,
660 2001.

661 Eresmaa, N., Karppinen, A., Joffre, S.M., Räsänen, J., Talvitie, H.: Mixing height
662 determination by ceilometer. *Atmos. Chem. Phys.* 6, 1485–1493. doi:10.5194/acp-6-1485-
663 2006, 2006.

664 Fujiwara, M., Sugidachi, T., Arai, T., Shimizu, K., Hayashi, M., Noma, Y., Kawagita, H.,
665 Sagara, K., Nakagawa, T., Okumura, S., Inai, Y., Shibata, T., Iwasaki, S., Shimizu, A.;
666 Development of a cloud particle sensor for radiosonde sounding. *Atmos. Meas. Tech.* 9,
667 5911–5931. doi:10.5194/amt-9-5911-2016, 2016.

668 Gambheer, A. V, Bhat, G.S.: Diurnal variation of deep cloud systems over the Indian region

669 using INSAT-1B pixel data. *Meteorol. Atmos. Phys.* 78, 215–225. doi:10.1007/s703-001-
670 8175-4, 2001.

671 George, G., Sarangi, C., Tripathi, S. N., Chakraborty, T., & Turner, A.: Vertical structure and
672 radiative forcing of monsoon clouds over Kanpur during the 2016 INCOMPASS field
673 campaign. *J. Geophys. Res.*, 123. <https://doi.org/10.1002/2017JD027759>, 2018.

674 Goloub, P., Deuze, J. L., Herman, M., and Fouquart, Y.: Analysis of the POLDER
675 polarization measurements performed over cloud covers, *IEEE T. Geosci. Remote*, 32, 78–
676 88, doi:10.1109/36.285191, 1994.

677 Hahn, C.J., Rossow, W.B., Warren, S.G.: ISCCP Cloud Properties Associated with Standard
678 Cloud Types Identified in Individual Surface Observations. *J. Clim.* 14, 11–28.
679 doi:10.1175/1520-0442(2001)014<0011:ICPAWS>2.0.CO;2, 2001.

680 Heintzenberg, J., Charlson, R.J. (Eds.): *Clouds in the perturbed climate system: their*
681 *relationship to energy balance, atmospheric dynamics and precipitation.* MIT Press,
682 Cambridge, UK, 2009.

683 Huang, Y.: On the Longwave Climate Feedbacks. *J. Clim.* 26, 7603–7610. doi:10.1175/JCLI-
684 D-13-00025.1, 2013.

685 Jiang, X., Waliser, D.E., Li, J.-L., Woods, C.: Vertical cloud structures of the boreal summer
686 intraseasonal variability based on CloudSat observations and ERA-interim reanalysis. *Clim.*
687 *Dyn.* 36, 2219–2232. doi:10.1007/s00382-010-0853-8, 2011.

688 Joiner, J. and Bhartia, P. K.: The determination of cloud pressures from rotational Raman
689 scattering in satellite backscatter ultraviolet measurements, *J. Geophys. Res.*, 100, 23019–
690 23026, doi:10.1029/95JD02675, 1995.

691 Kim, S.-W., Chung, E.-S., Yoon, S.-C., Sohn, B.-J., Sugimoto, N.: Intercomparisons of
692 cloud-top and cloud-base heights from ground-based Lidar, CloudSat and CALIPSO
693 measurements. *Int. J. Remote Sens.* 32, 1179–1197. doi:10.1080/01431160903527439, 2011.

694 Lazarus, S.M., Krueger, S.K., Mace, G.G.: A Cloud Climatology of the Southern Great Plains
695 ARM CART. J. Clim. 13, 1762–1775. doi:10.1175/1520-
696 0442(2000)013<1762:ACCOTS>2.0.CO;2, 2000.

697 King, N. J. and Vaughan, G.: Using passive remote sensing to retrieve the vertical variation
698 of cloud droplet size in marine stratocumulus: An assessment of information content and the
699 potential for improved retrievals from hyperspectral measurements, *J. Geophys. Res.*, 117,
700 D15206, doi:10.1029/2012JD017896, 2012.

701 Knibbe, W. J. J., De Haan, J. F., Hovenier, J. W., Stam, D. M., Koelemeijer, R. B. A., and
702 Stammes, P.: Deriving terrestrial cloud top pressure from photopolarimetry of reflected light,
703 *J. Quant. Spectrosc. Ra.*, 64, 173–199, doi:10.1016/S0022-4073(98)00135-6, 2000.

704 L'Ecuyer, T. ~S., Jiang, J. ~H.: Touring the atmosphere aboard the A-Train. *Phys. Today* 63,
705 36. doi:10.1063/1.3463626, 2010.

706 Li, J., Yi, Y., Minnis, P., Huang, J., Yan, H., Ma, Y., Wang, W., Kirk Ayers, J.: Radiative
707 effect differences between multi-layered and single-layer clouds derived from CERES,
708 CALIPSO, and CloudSat data. *J. Quant. Spectrosc. Radiat. Transf.* 112, 361–375.
709 doi:<https://doi.org/10.1016/j.jqsrt.2010.10.006>, 2011.

710 Li, Y., Liu, X., Chen, B.: Cloud type climatology over the Tibetan Plateau: A comparison of
711 ISCCP and MODIS/TERRA measurements with surface observations. *Geophys. Res. Lett.*
712 33, n/a-n/a. doi:10.1029/2006GL026890, 2006.

713 Li, Z., Barker, H.W., Moreau, L.: The variable effect of clouds on atmospheric absorption of
714 solar radiation. *Nature* 376, 486–490, 1995.

715 Li, Z., Cribb, M.C., Chang, F.-L., Trishchenko, A., Luo, Y.: Natural variability and sampling
716 errors in solar radiation measurements for model validation over the Atmospheric Radiation
717 Measurement Southern Great Plains region. *J. Geophys. Res. Atmos.* 110, n/a-n/a.

718 doi:10.1029/2004JD005028, 2005.

719 Luo, Y., Zhang, R., Wang, H.: Comparing Occurrences and Vertical Structures of
720 Hydrometeors between Eastern China and the Indian Monsoon Region Using
721 CloudSat/CALIPSO Data. *J. Clim.* 22, 1052–1064. doi:10.1175/2008JCLI2606.1, 2009.

722 Merlin, G., Riedi, J., Labonnote, L. C., Cornet, C., Davis, A. B., Dubuisson, P., Desmons,
723 M., Ferlay, N., and Parol, F.: Cloud information content analysis of multi-angular
724 measurements in the oxygen A-band: application to 3MI and MSPI, *Atmos. Meas. Tech.*, 9,
725 4977-4995, doi:amt-9-4977-2016, 2016.

726 Minnis, P., Yi, Y., Huang, J., Ayers, K.: Relationships between radiosonde and RUC-2
727 meteorological conditions and cloud occurrence determined from ARM data. *J. Geophys.*
728 *Res. Atmos.* 110, n/a-n/a. doi:10.1029/2005JD006005, 2005.

729 Moroney, C., Davies, R., and Muller, J.-P.: Operational retrieval of cloud-top heights using
730 MISR data, *IEEE T. Geosci. Remote*, 40, 1532–1540, doi:10.1109/TGRS.2002.801150,
731 2002.

732 Nath, D., Venkat Ratnam, M., Jagannadha Rao, V.V.M., Krishna Murthy, B. V, Vijaya
733 Bhaskara Rao, S.: Gravity wave characteristics observed over a tropical station using high-
734 resolution GPS radiosonde soundings. *J. Geophys. Res. Atmos.* 114, n/a-n/a.
735 doi:10.1029/2008JD011056, 2009.

736 Naud, C.M., Chen, Y.-H.: Assessment of ISCCP cloudiness over the Tibetan Plateau using
737 CloudSat-CALIPSO. *J. Geophys. Res. Atmos.* 115, n/a-n/a. doi:10.1029/2009JD013053,
738 2010.

739 Naud, C.M., Muller, J.-P., Clothiaux, E.E.: Comparison between active sensor and
740 radiosonde cloud boundaries over the ARM Southern Great Plains site. *J. Geophys. Res.*
741 *Atmos.* 108, n/a-n/a. doi:10.1029/2002JD002887, 2003.

742 Noh, Y.-J., Seaman, C.J., Vonder Haar, T.H., Hudak, D.R., Rodriguez, P.: Comparisons and

743 analyses of aircraft and satellite observations for wintertime mixed-phase clouds. *J. Geophys.*
744 *Res. Atmos.* 116, n/a-n/a. doi:10.1029/2010JD015420, 2011.

745 Nowak, D., Ruffieux, D., Agnew, J.L., Vuilleumier, L.: Detection of Fog and Low Cloud
746 Boundaries with Ground-Based Remote Sensing Systems. *J. Atmos. Ocean. Technol.* 25,
747 1357–1368. doi:10.1175/2007JTECHA950.1, 2008.

748 Pallamraju, D., Gurubaran, S., Venkat Ratnam, M.: A brief overview on the special issue on
749 CAWSES-India Phase II program. *J. Atmos. Solar-Terrestrial Phys.* 121, 141–144.
750 doi:https://doi.org/10.1016/j.jastp.2014.10.013, 2014.

751 Platnick, S., King, M. D., Ackerman, S., Menzel, W. P., Baum, B., Riedi, J. C., and Frey, R.:
752 The MODIS cloud products: Algorithms and examples from Terra, *IEEE T. Geosci. Remote*,
753 41, 459–473, doi:10.1109/TGRS.2002.808301, 2003.

754 Poore, K.D., Wang, J., Rossow, W.B.: Cloud Layer Thicknesses from a Combination of
755 Surface and Upper-Air Observations. *J. Clim.* 8, 550–568. doi:10.1175/1520-
756 0442(1995)008<0550:CLTFAC>2.0.CO;2, 1995.

757 Qian, Y., Long, C.N., Wang, H., Comstock, J.M., McFarlane, S.A., Xie, S.: Evaluation of
758 cloud fraction and its radiative effect simulated by IPCC AR4 global models against ARM
759 surface observations. *Atmos. Chem. Phys.* 12, 1785–1810. doi:10.5194/acp-12-1785-2012,
760 2012.

761 Ramanathan, V., Cess, R.D., Harrison, E.F., Minnis, P., Barkstorm, B.R., Ahmad, E.,
762 Hartmann, D.: Cloud-Radiative Forcing and Climate: Results from the Earth Radiation
763 Budget Experiment. *Science (80-.)*. 243, 57 LP-63,, 1989.

764 Randall, D.A.: Cloud parameterization for climate modeling: Status and prospects. *Atmos.*
765 *Res.* 23, 345–361. doi:https://doi.org/10.1016/0169-8095(89)90025-2, 1989.

766 Rao, T.N., Kirankumar, N.V.P., Radhakrishna, B., Rao, D.N., Nakamura, K.: Classification
767 of Tropical Precipitating Systems Using Wind Profiler Spectral Moments. Part II: Statistical

768 Characteristics of Rainfall Systems and Sensitivity Analysis. *J. Atmos. Ocean. Technol.* 25,
769 898–908. doi:10.1175/2007JTECHA1032.1, 2008a.

770 Ravi Kiran, V., Rajeevan, M., Gadhavi, H., Rao, S.V.B., Jayaraman, A.: Role of vertical
771 structure of cloud microphysical properties on cloud radiative forcing over the Asian
772 monsoon region. *Clim. Dyn.* 45, 3331–3345. doi:10.1007/s00382-015-2542-0, 2015.

773 Reddy, N.N., Rao, K.G.: Contrasting variations in the surface layer structure between the
774 convective and non-convective periods in the summer monsoon season for Bangalore
775 location during PRWONAM. *J. Atmos. Solar-Terrestrial Phys.* 167, 156-168.
776 doi:10.1016/j.jastp.2017.11.017, 2017, 2018.

777 Rind, D., Rossow, W.B.: The Effects of Physical Processes on the Hadley Circulation. *J.*
778 *Atmos. Sci.* 41, 479–507. doi:10.1175/1520-0469(1984)041<0479:TEOPPO>2.0.CO;2,
779 1984.

780 Roja Raman, M., Jagannadha Rao, V.V.M., Venkat Ratnam, M., Rajeevan, M., Rao, S.V.B.,
781 Narayana Rao, D., Prabhakara Rao, N.: Characteristics of the Tropical Easterly Jet: Long-
782 term trends and their features during active and break monsoon phases. *J. Geophys. Res.*
783 *Atmos.* 114, n/a-n/a. doi:10.1029/2009JD012065, 2009.

784 Rossow, W. B. and Schiffer, R. A.: ISCCP Cloud Data Products, *B. Am. Meteorol. Soc.*, 72,
785 2–20, doi:10.1175/1520-0477(1991)072<0002:ICDP>2.0.CO;2, 1991.

786 Rossow, W.B., Garder, L.C.: Validation of ISCCP Cloud Detections. *J. Clim.* 6, 2370–2393.
787 doi:10.1175/1520-0442(1993)006<2370:VOICD>2.0.CO;2, 1993.

788 Rossow, W.B., Lacis, A.A.: Global, Seasonal Cloud Variations from Satellite Radiance
789 Measurements. Part II. Cloud Properties and Radiative Effects. *J. Clim.* 3, 1204–1253.
790 doi:10.1175/1520-0442(1990)003<1204:GSCVFS>2.0.CO;2, 1990.

791 Rossow, W.B., Zhang, Y.: Evaluation of a Statistical Model of Cloud Vertical Structure
792 Using Combined CloudSat and CALIPSO Cloud Layer Profiles. *J. Clim.* 23, 6641–6653.

793 doi:10.1175/2010JCLI3734.1, 2010.

794 Rossow, W.B., Zhang, Y., Wang, J.: A Statistical Model of Cloud Vertical Structure Based
795 on Reconciling Cloud Layer Amounts Inferred from Satellites and Radiosonde Humidity
796 Profiles. *J. Clim.* 18, 3587–3605. doi:10.1175/JCLI3479.1, 2005.

797 Sassen, K., Wang, Z.: Classifying clouds around the globe with the CloudSat radar: 1-year of
798 results. *Geophys. Res. Lett.* 35, n/a-n/a. doi:10.1029/2007GL032591, 2008.

799 Seiz, G., Tjemkes, S., and Watts, P.: Multiview Cloud-Top Height and Wind Retrieval with
800 Photogrammetric Methods: Application to Meteosat-8 HRV Observations, *J. Appl. Meteorol.*
801 *Clim.*, 46,1182–1195, doi:10.1175/JAM2532.1, 2007.

802 Slingo, A., Slingo, J.M.: The response of a general circulation model to cloud longwave
803 radiative forcing. I: Introduction and initial experiments. *Q. J. R. Meteorol. Soc.* 114, 1027–
804 1062. doi:10.1002/qj.49711448209, 1988.

805 Slingo, J.M., Slingo, A.: The response of a general circulation model to cloud longwave
806 radiative forcing. II: Further studies. *Q. J. R. Meteorol. Soc.* 117, 333–364.
807 doi:10.1002/qj.49711749805, 1991.

808 Stephens, G.L.: Cloud Feedbacks in the Climate System: A Critical Review. *J. Clim.* 18,
809 237–273. doi:10.1175/JCLI-3243.1, 2005.

810 Stephens, G.L., Vane, D.G., Tanelli, S., Im, E., Durden, S., Rokey, M., Reinke, D., Partain,
811 P., Mace, G.G., Austin, R., L’Ecuyer, T., Haynes, J., Lebsock, M., Suzuki, K., Waliser, D.,
812 Wu, D., Kay, J., Gettelman, A., Wang, Z., Marchand, R.: CloudSat mission: Performance and
813 early science after the first year of operation. *J. Geophys. Res. Atmos.* 113, n/a-n/a.
814 doi:10.1029/2008JD009982, 2008.

815 Subrahmanyam, K.V., Kumar, K.K.: CloudSat observations of multi layered clouds across
816 the globe. *Clim. Dyn.* 49, 327–341. doi:10.1007/s00382-016-3345-7, 2017.

817 Uma, K.N., Kumar, K.K., Shankar Das, S., Rao, T.N., Satyanarayana, T.M.: On the Vertical

818 Distribution of Mean Vertical Velocities in the Convective Regions during the Wet and Dry
819 Spells of the Monsoon over Gadanki. *Mon. Weather Rev.* 140, 398–410. doi:10.1175/MWR-
820 D-11-00044.1, 2012.

821 Venkat Ratnam, M., Narendra Babu, A., Jagannadha Rao, V.V.M., Vijaya Bhaskar Rao, S.,
822 Narayana Rao, D.: MST radar and radiosonde observations of inertia-gravity wave
823 climatology over tropical stations: Source mechanisms. *J. Geophys. Res. Atmos.* 113, n/a-n/a.
824 doi:10.1029/2007JD008986, 2008.

825 Venkat Ratnam, M., Pravallika, N., Ravindra Babu, S., Basha, G., Pramitha, M., Krishna
826 Murthy, B. V.: Assessment of GPS radiosonde descent data. *Atmos. Meas. Tech.* 7, 1011–
827 1025. doi:10.5194/amt-7-1011-2014, 2014a.

828 Venkat Ratnam, M., Sunilkumar, S. V., Parameswaran, K., Krishna Murthy, B. V.,
829 Ramkumar, G., Rajeev, K., Basha, G., Ravindra Babu, S., Muhsin, M., Kumar Mishra, M.,
830 Hemanth Kumar, A., Akhil Raj, S.T., Pramitha, M.: Tropical tropopause dynamics (TTD)
831 campaigns over Indian region: An overview. *J. Atmos. Solar-Terrestrial Phys.* 121, 229–239.
832 doi:<https://doi.org/10.1016/j.jastp.2014.05.007>, 2014b.

833 Wang, F., Xin, X., Wang, Z., Cheng, Y., Zhang, J., Yang, S.: Evaluation of cloud vertical
834 structure simulated by recent BCC_AGCM versions through comparison with CALIPSO-
835 GOCCP data. *Adv. Atmos. Sci.* 31, 721–733. doi:10.1007/s00376-013-3099-7, 2014.

836 Wang, J., Rossow, W.B.: Effects of Cloud Vertical Structure on Atmospheric Circulation in
837 the GISS GCM. *J. Clim.* 11, 3010–3029. doi:10.1175/1520-
838 0442(1998)011<3010:EOCVSO>2.0.CO;2, 1998.

839 Wang, J., Rossow, W.B.: Determination of Cloud Vertical Structure from Upper-Air
840 Observations. *J. Appl. Meteorol.* 34, 2243–2258. doi:10.1175/1520-
841 0450(1995)034<2243:DOCVSF>2.0.CO;2, 1995.

842 Wang, J., Rossow, W.B., Uttal, T., Rozendaal, M.: Variability of Cloud Vertical Structure

843 during ASTEX Observed from a Combination of Rawinsonde, Radar, Ceilometer, and
844 Satellite. *Mon. Weather Rev.* 127, 2484–2502. doi:10.1175/1520-
845 0493(1999)127<2484:VOCVSD>2.0.CO;2, 1999.

846 Wang, J., Rossow, W.B., Zhang, Y.: Cloud Vertical Structure and Its Variations from a 20-Yr
847 Global Rawinsonde Dataset. *J. Clim.* 13, 3041–3056. doi:10.1175/1520-
848 0442(2000)013<3041:CVSAIV>2.0.CO;2, 2000.

849 Warren, S.G., Hahn, C.J., London, J., Chervin, R.M., Jenne, R.L.: Global distribution of total
850 cloud cover and cloud type amounts over the ocean. doi:TN-317+STR, 212 pp, 1988.

851 Wielicki, B.A., Harrison, E.F., Cess, R.D., King, M.D., Randall, D.A. Mission to Planet
852 Earth: Role of Clouds and Radiation in Climate. *Bull. Am. Meteorol. Soc.* 76, 2125–2153.
853 doi:10.1175/1520-0477(1995)076<2125:MTPERO>2.0.CO;2, 1995.

854 Winker, D.M., Hunt, W.H., McGill, M.J.; Initial performance assessment of CALIOP.
855 *Geophys. Res. Lett.* 34, n/a-n/a. doi:10.1029/2007GL030135, 2007.

856 Wu, D. L., Ackerman, S. a., Davies, R., Diner, D. J., Garay, M. J., Kahn, B. H., Maddux, B.
857 C., Moroney, C. M., Stephens, G. L., Veefkind, J. P., and Vaughan, M. A.: Vertical
858 distributions and relationships of cloud occurrence frequency as observed by MISR, AIRS,
859 MODIS, OMI, CALIPSO, and CloudSat, *Geophys. Res. Lett.*, 36, L09821,
860 doi:10.1029/2009GL037464, 2009.

861 Xi, B., Dong, X., Minnis, P., Khaiyer, M.M.: A 10 year climatology of cloud fraction and
862 vertical distribution derived from both surface and GOES observations over the DOE ARM
863 SPG site. *J. Geophys. Res. Atmos.* 115, n/a-n/a. doi:10.1029/2009JD012800, 2010.

864 Yang, Q., Fu, Q., Hu, Y.: Radiative impacts of clouds in the tropical tropopause layer. *J.*
865 *Geophys. Res. Atmos.* 115, n/a-n/a. doi:10.1029/2009JD012393, 2010.

866 Zhang, J., Chen, H., Li, Z., Fan, X., Peng, L., Yu, Y., Cribb, M.: Analysis of cloud layer
867 structure in Shouxian, China using RS92 radiosonde aided by 95 GHz cloud radar. *J.*

868 Geophys. Res. Atmos. 115, n/a-n/a. doi:10.1029/2010JD014030, 2010.

869 Zuidema, P.: Convective Clouds over the Bay of Bengal. Mon. Weather Rev. 131, 780–798.

870 doi:10.1175/1520-0493(2003)131<0780:CCOTBO>2.0.CO;2, 2003.

871 **Tables:**

872

	Height-resolving RH thresholds		
Altitude range	min-RH	max-RH	inter-RH
0-2 km	92%	95%	84%
2-6 km	90%	93%	82%
6-12 km	88%	90%	78%
>12 km	75%	80%	70%

873

874 **Table 1.** Summary of height-resolving RH thresholds.

875

	Multi-layer clouds	Cloud base altitude (km)	Cloud top altitude (km)	Cloud thickness (km)
	Single-layer cloud	6.32	9.24	2.92
Upper layer	two-layer clouds	8.51	11.23	2.72
	three-layer clouds	9.63	11.79	2.16
Middle layer	three-layer clouds	6.69	7.80	1.11
Lower layer	two-layer clouds	4.08	5.56	1.48
	three-layer clouds	3.04	4.31	1.27

876

877 **Table 2.** Mean base, top and thicknesses of cloud layers of single-layer, two-layer and three-
878 layer clouds.

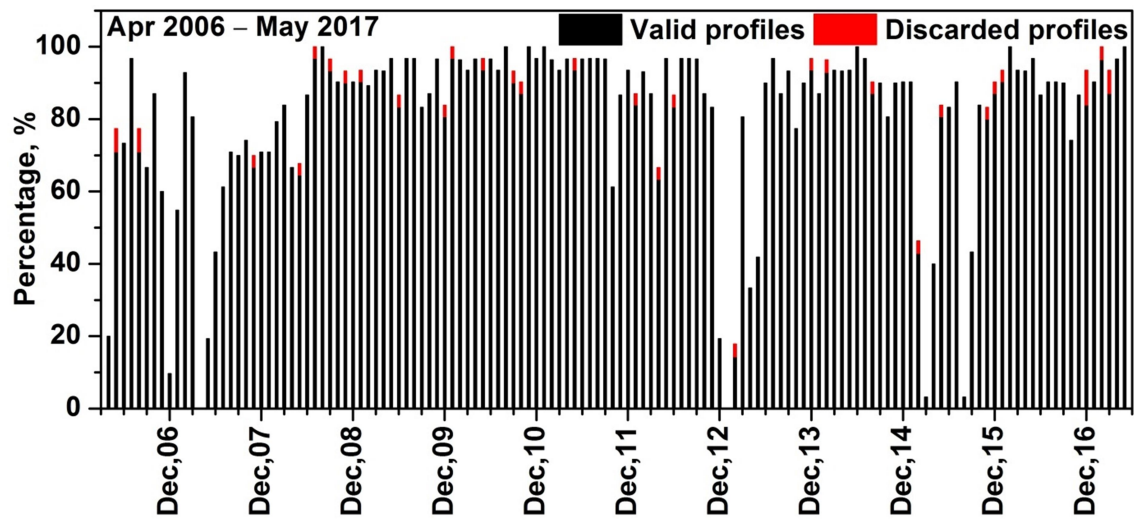
879

880

881

882 **Figures:**

883



884

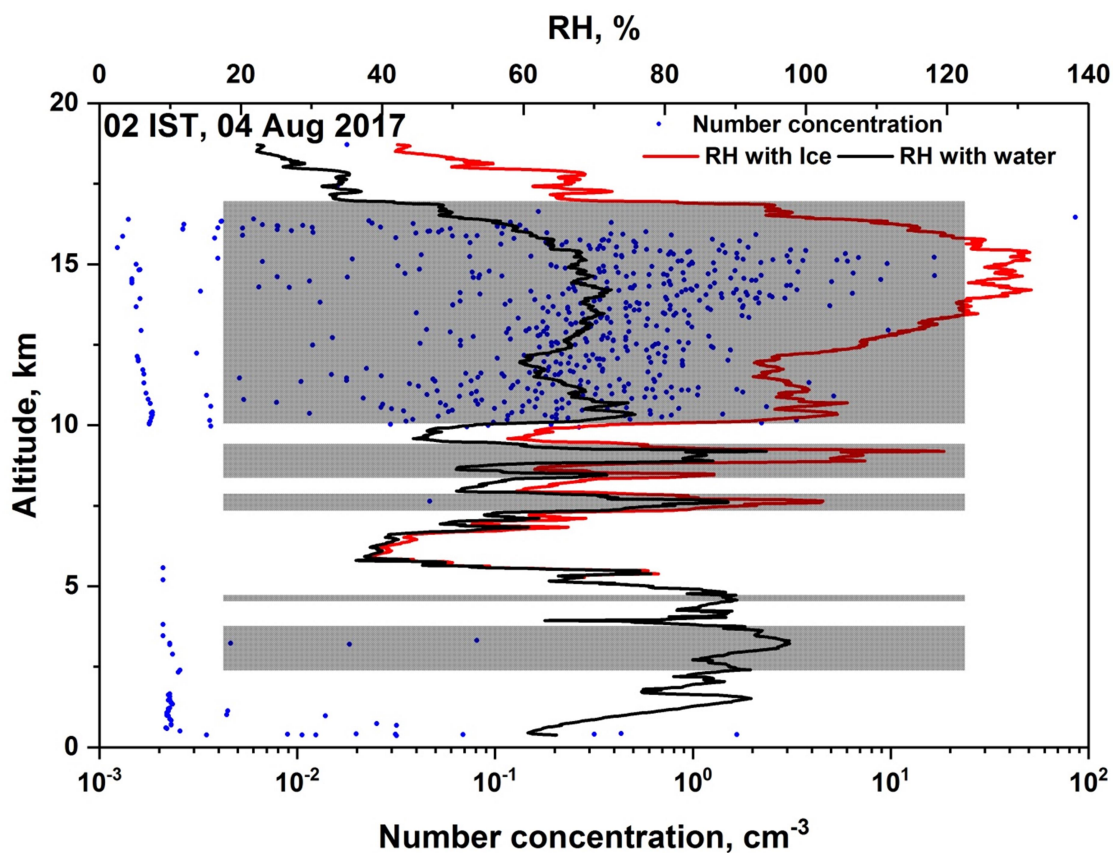
885 **Figure 1.** Monthly percentage of radiosonde data available during Apr. 2006 – May 2017 at

886 Gadanki. Percentage of discarded profiles in each month is also shown with red colour.

887

888

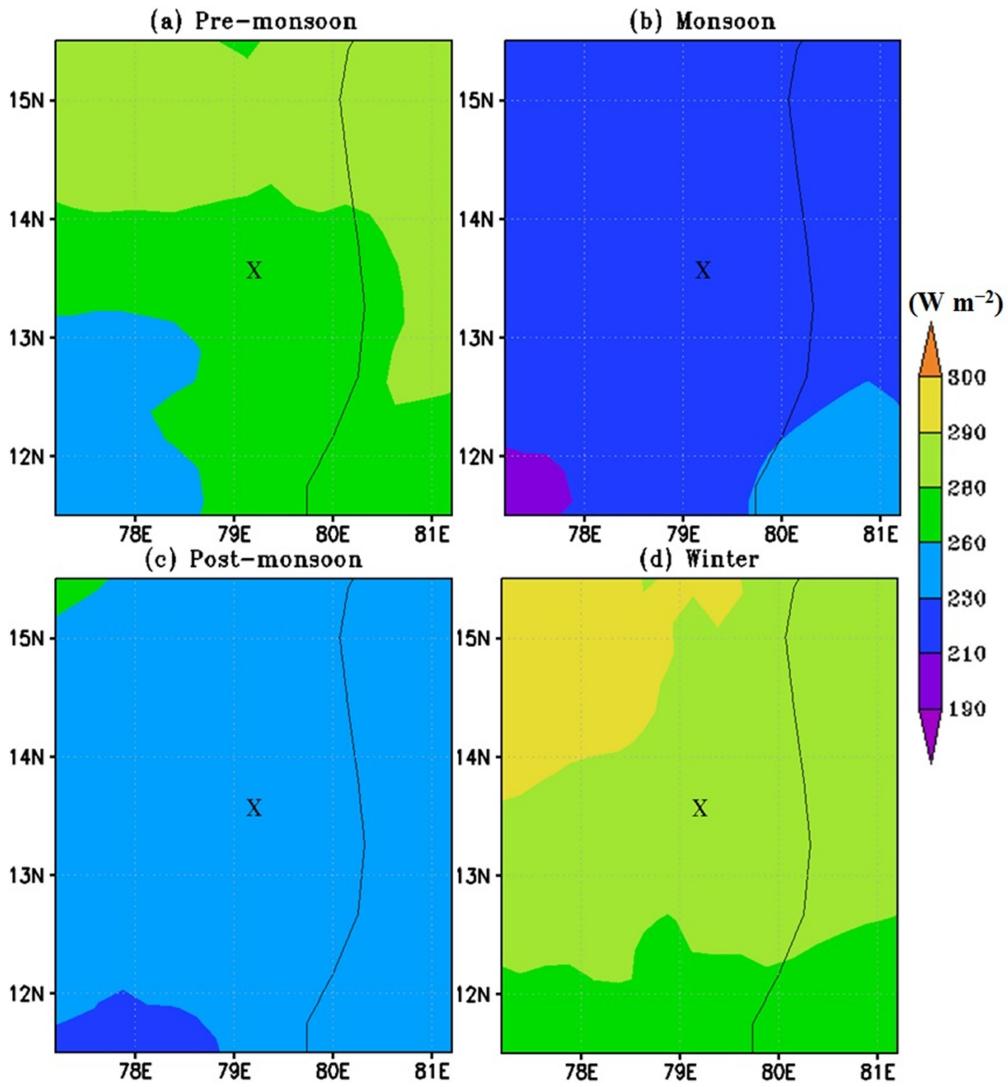
889



890

891 **Figure 2.** Results from a flight of RS-11G radiosonde and Cloud Particle Sensor (CPS) sonde
892 on the same balloon launched at 02 IST on 04 Aug, 2017 at Gadanki, India. Profiles of RH
893 estimated with respect to water (black solid line) and ice (when temperatures are less than
894 0°C (red solid line)), and number concentration (filled blue circles) from CPS sonde profile
895 are shown. Detected cloud layer boundaries are shown by the filled gray rectangle boxes.
896 Increase in the number concentration within the detected cloud layers indicates the cloud
897 layer boundaries detected in the present study are accurate.

898



899

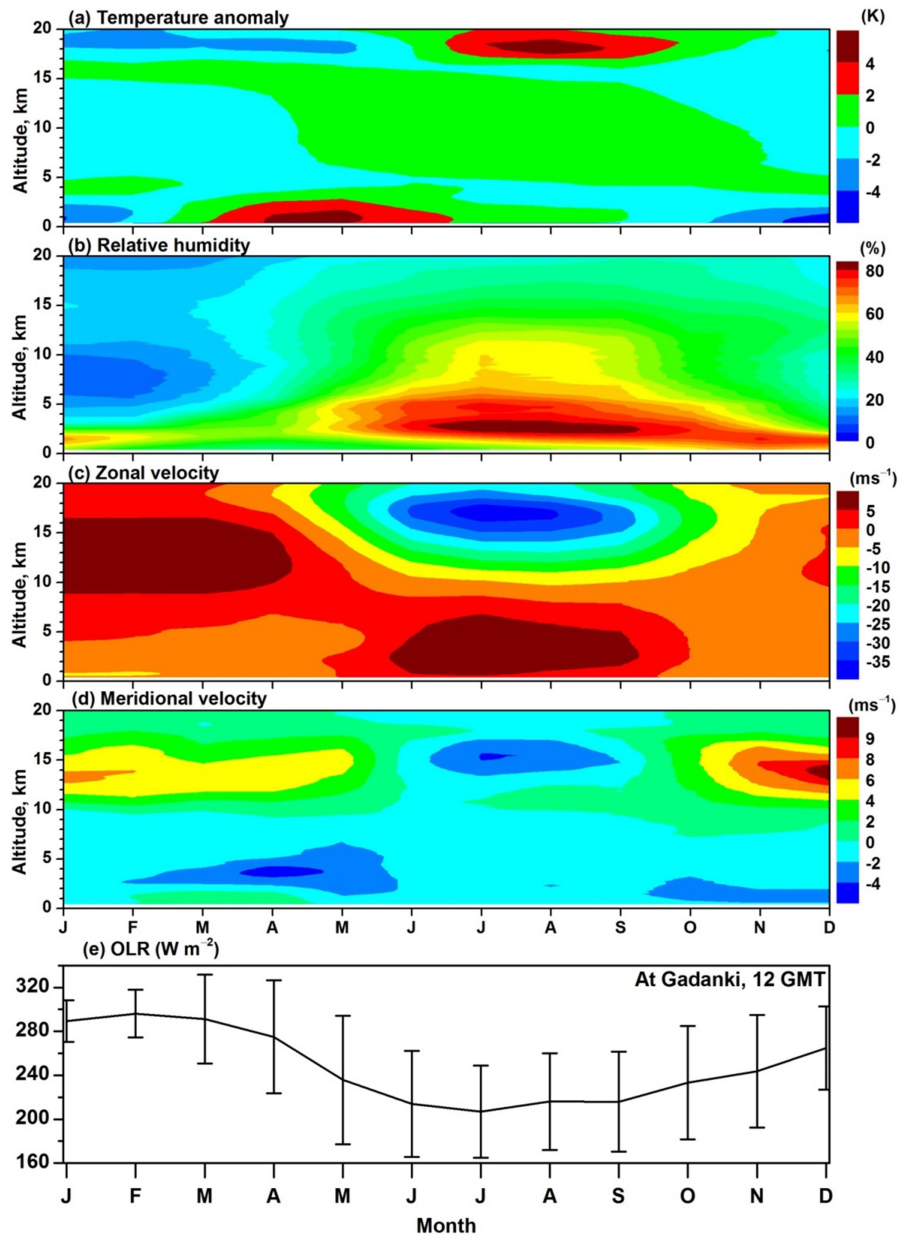
900

901 **Figure 3.** Seasonal mean distribution of OLR around Gadanki location observed during (a)

902 Pre-monsoon, (b) Monsoon, (c) Post-monsoon and (d) Winter seasons averaged during

903 2006 – 2017. The symbol ‘X’ indicates the location of Gadanki.

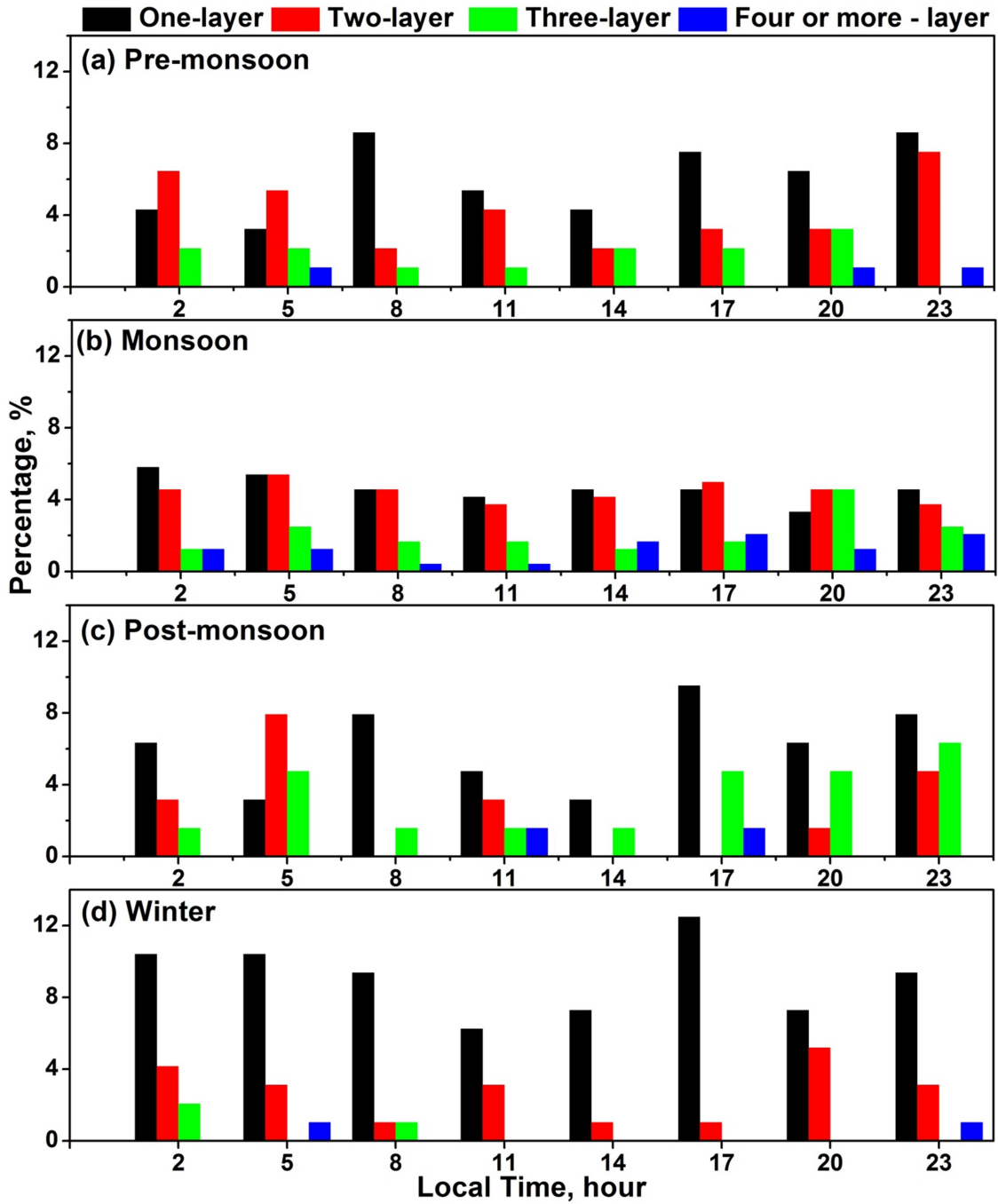
904



905

906 **Figure 4.** Time–altitude cross sections of monthly mean (a) Temperature anomaly, (b)
 907 Relative humidity, (c) Zonal wind and (d) Meridional wind observed over Gadanki using
 908 radiosonde observations during Apr. 2006 to May 2017. (e) Monthly mean Outgoing
 909 Longwave Radiation (OLR) over Gadanki obtained using KALPANA-1 data during Apr.
 910 2006 to May 2017 along with standard deviation (vertical bars).

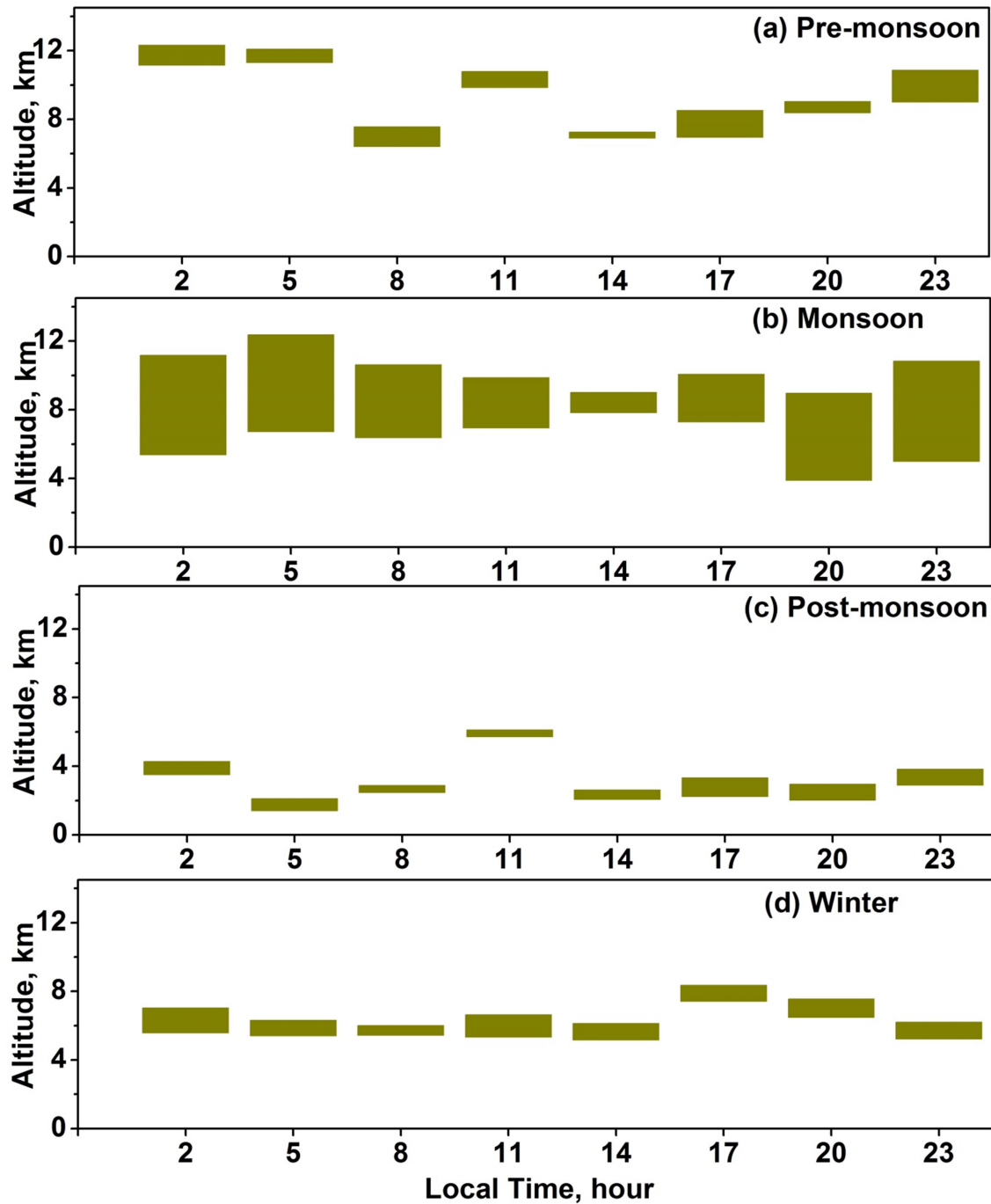
911



912

913 **Figure 5.** Diurnal variations of one-layer, two-layer, three-layer, and four- or more- layer
 914 clouds observed during (a) pre-monsoon, (b) monsoon, (c) post-monsoon, and (d) winter
 915 seasons.

916



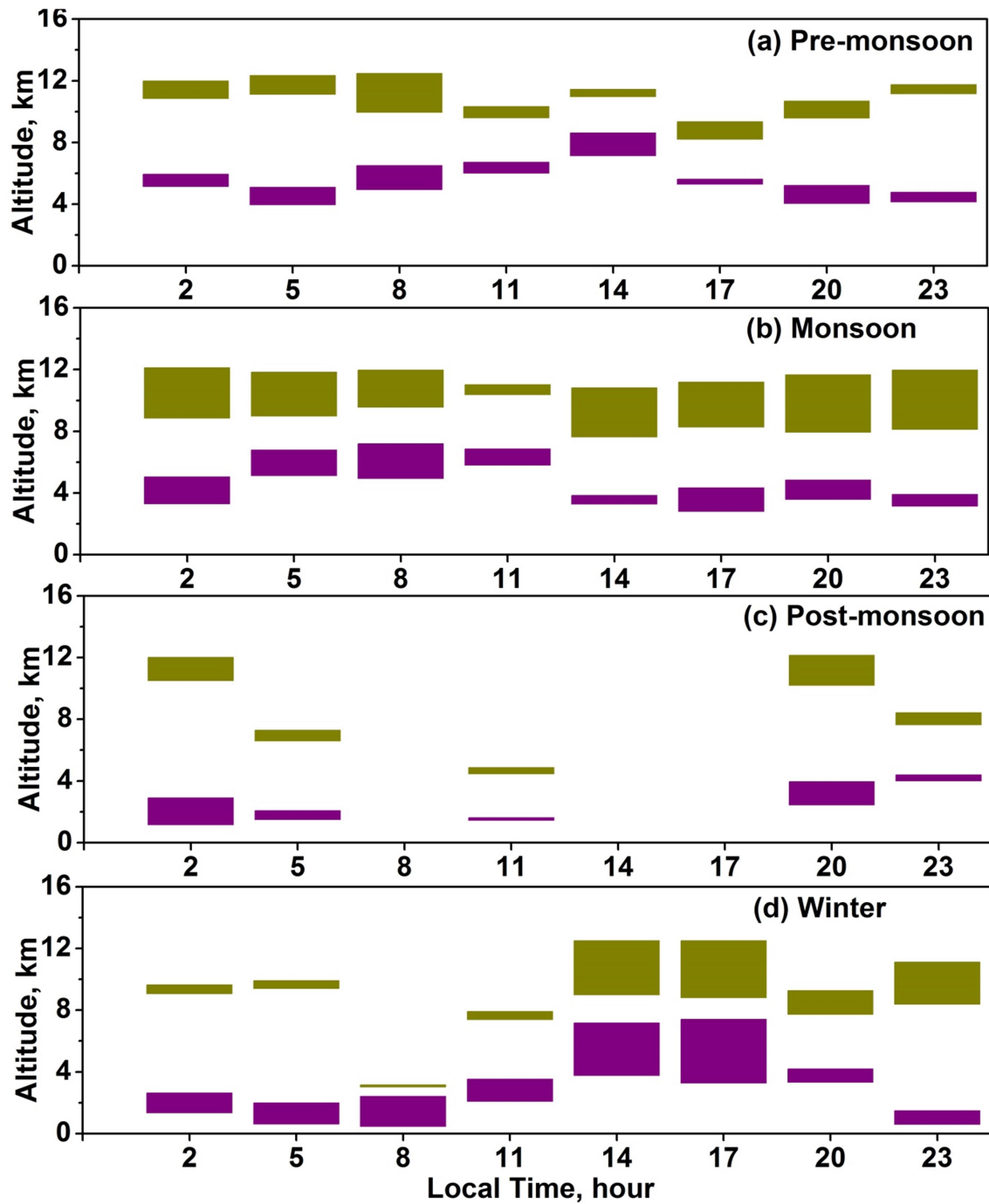
917

918 **Figure 6.** Diurnal variations of mean vertical locations (base and top), thicknesses of one-

919 layer clouds observed during (a) pre-monsoon, (b) monsoon, (c) post-monsoon, and (d)

920 winter seasons.

921

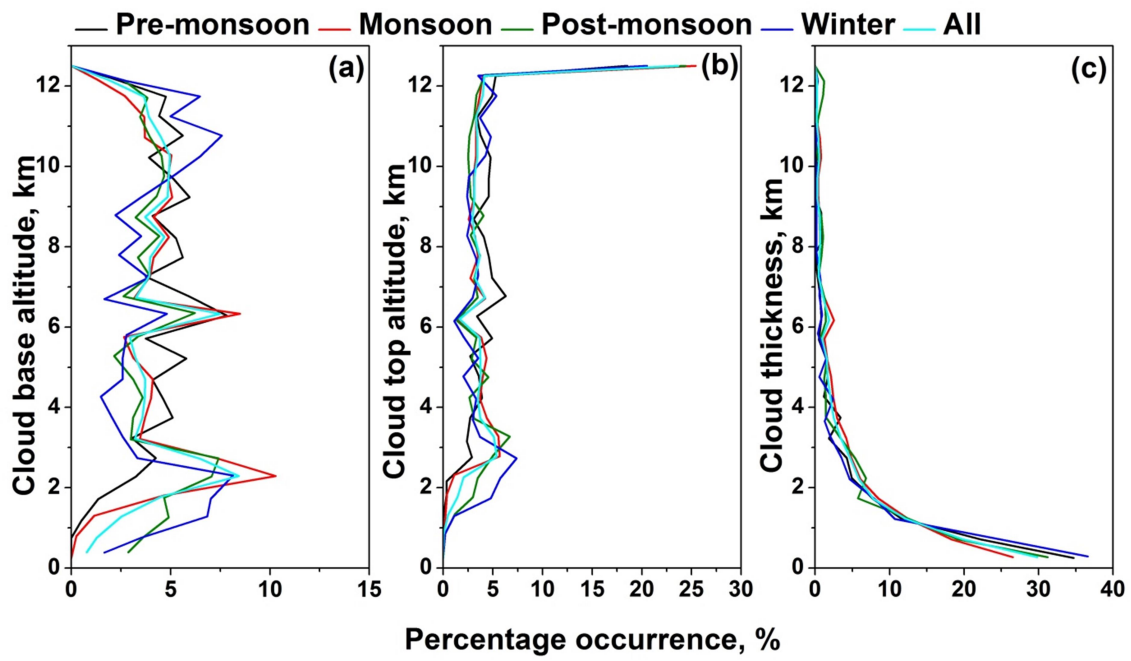


922

923 **Figure 7.** Diurnal variations of mean vertical locations (base and top), thicknesses of two-
 924 layer clouds observed during (a) pre-monsoon, (b) monsoon, (c) post-monsoon, and (d)
 925 winter seasons.

926

927



929

930 **Figure 8.** Percentage occurrence of the (a) cloud base altitude, (b) cloud top altitude and (c)

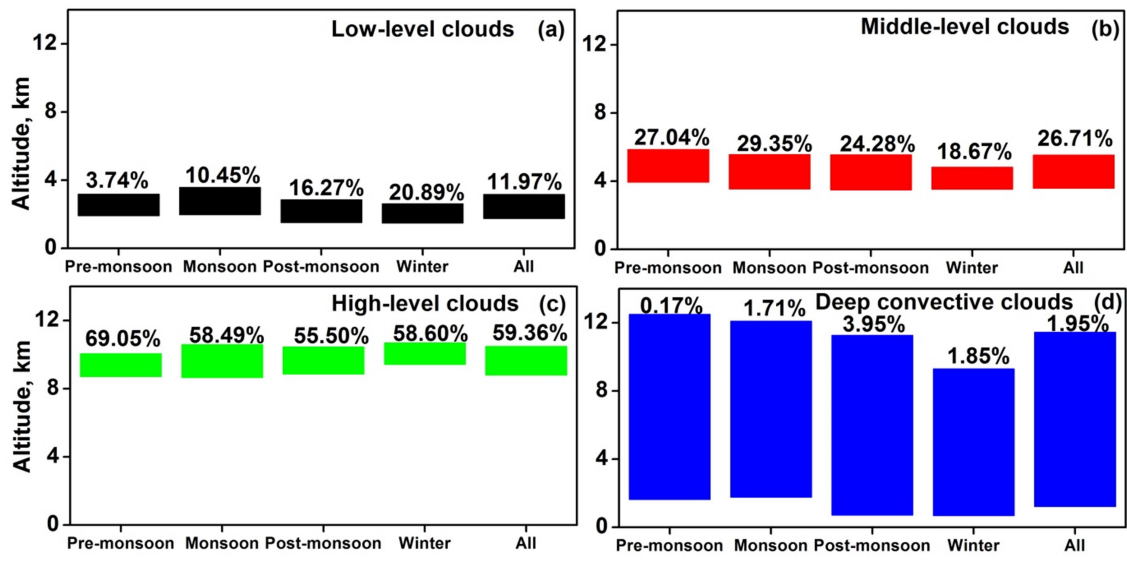
931 cloud thickness observed during different seasons over Gadanki. Altitude bin size is 500 m.

932

933

934

935



936

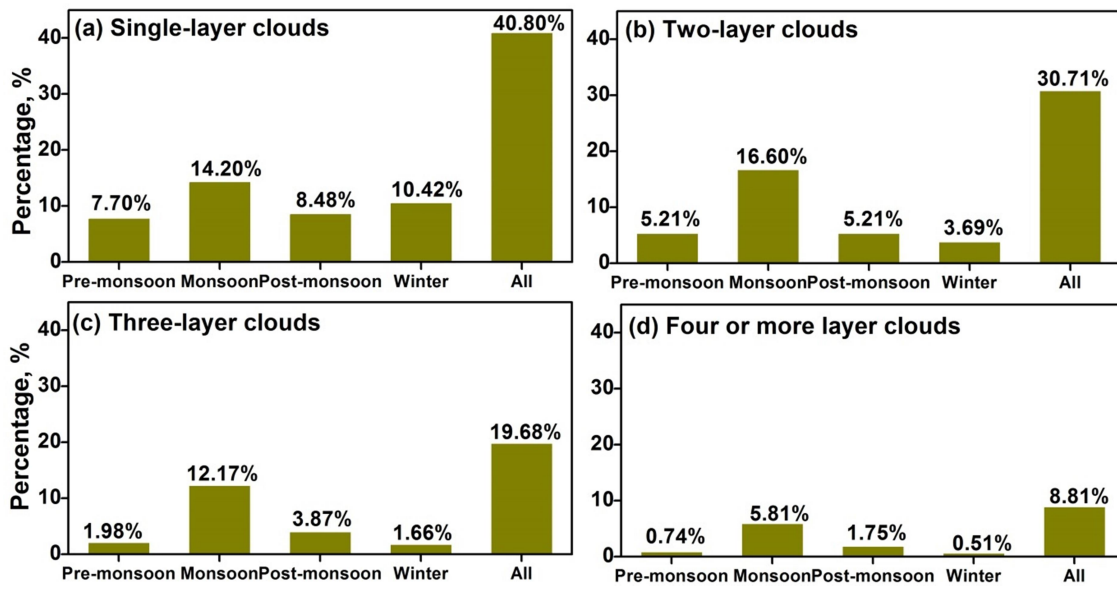
937

938 **Figure 9.** Mean vertical locations (base and top), cloud thicknesses and percentage
939 occurrence of (a) low-level clouds, (b) middle-level clouds, (c) high-level clouds and (d)
940 Deep convective clouds observed during different seasons.

941

942

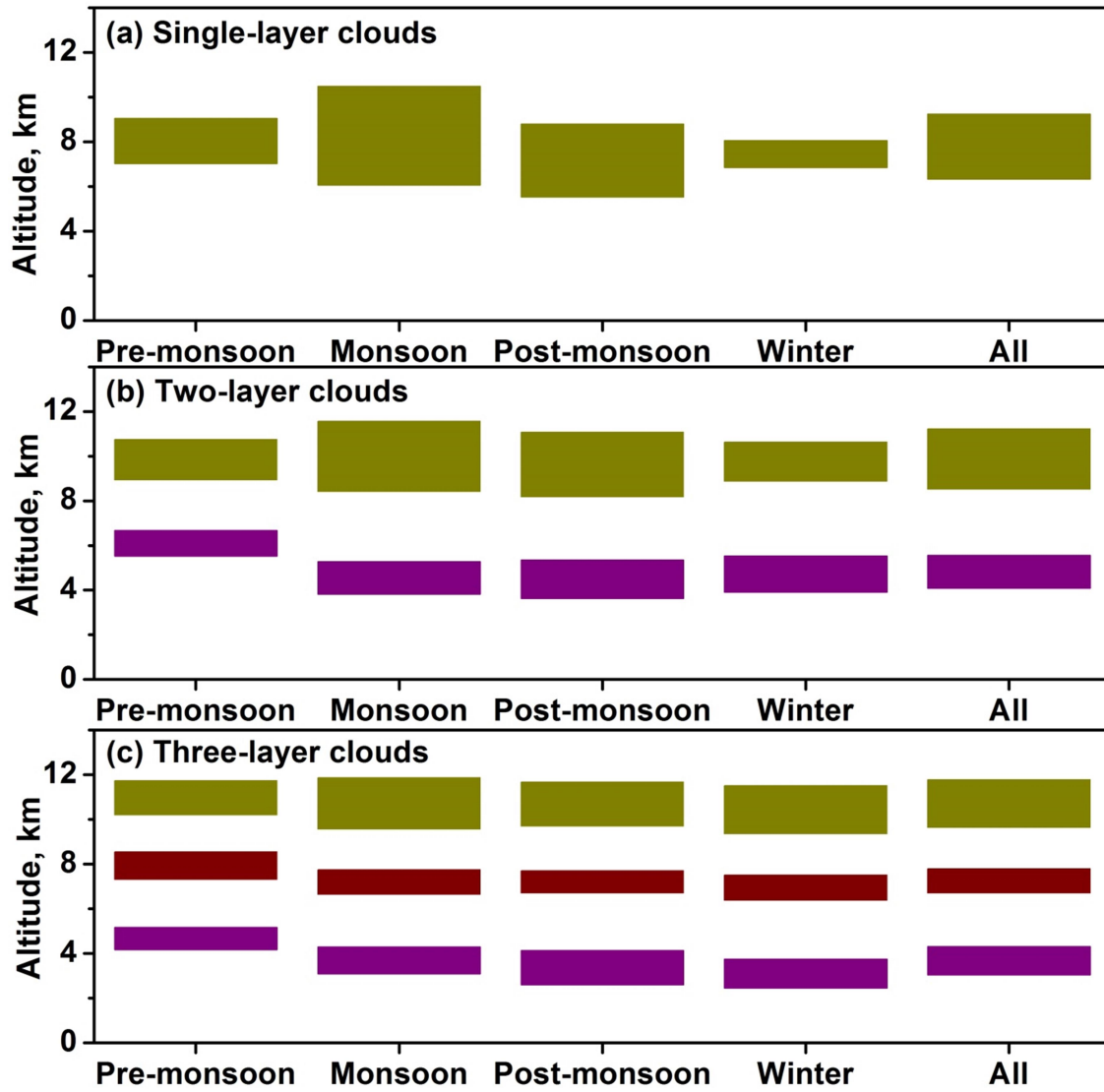
943



944

945 **Figure 10.** Percentage occurrence of (a) one-layer, (b) two-layer, (c) three-layer, and (d)
946 four- or more- layer clouds observed during different seasons.

947



948

949

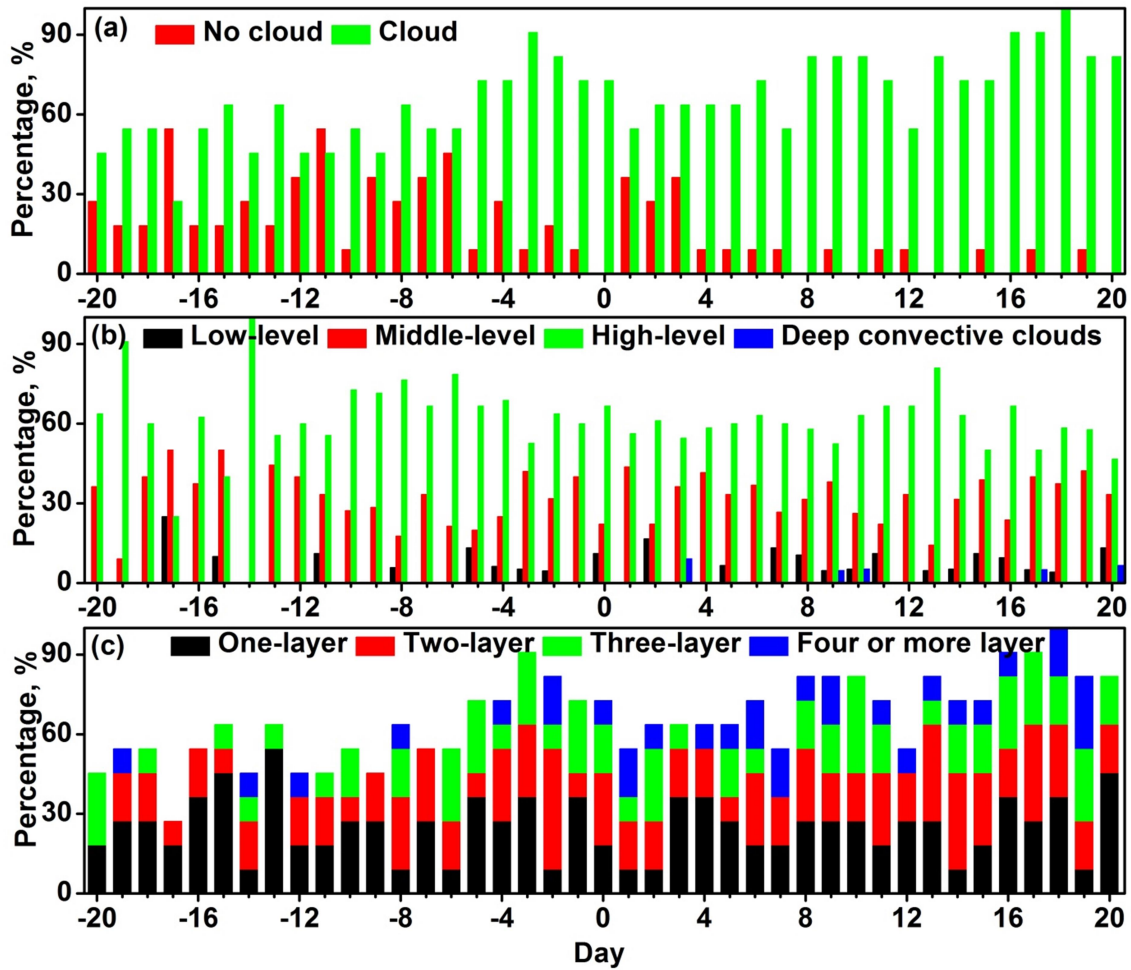
950 **Figure 11.** Mean vertical locations (base and top), cloud thicknesses of (a) one-layer clouds,

951 (b) two-layer clouds, (c) three-layer clouds observed during different seasons.

952

953

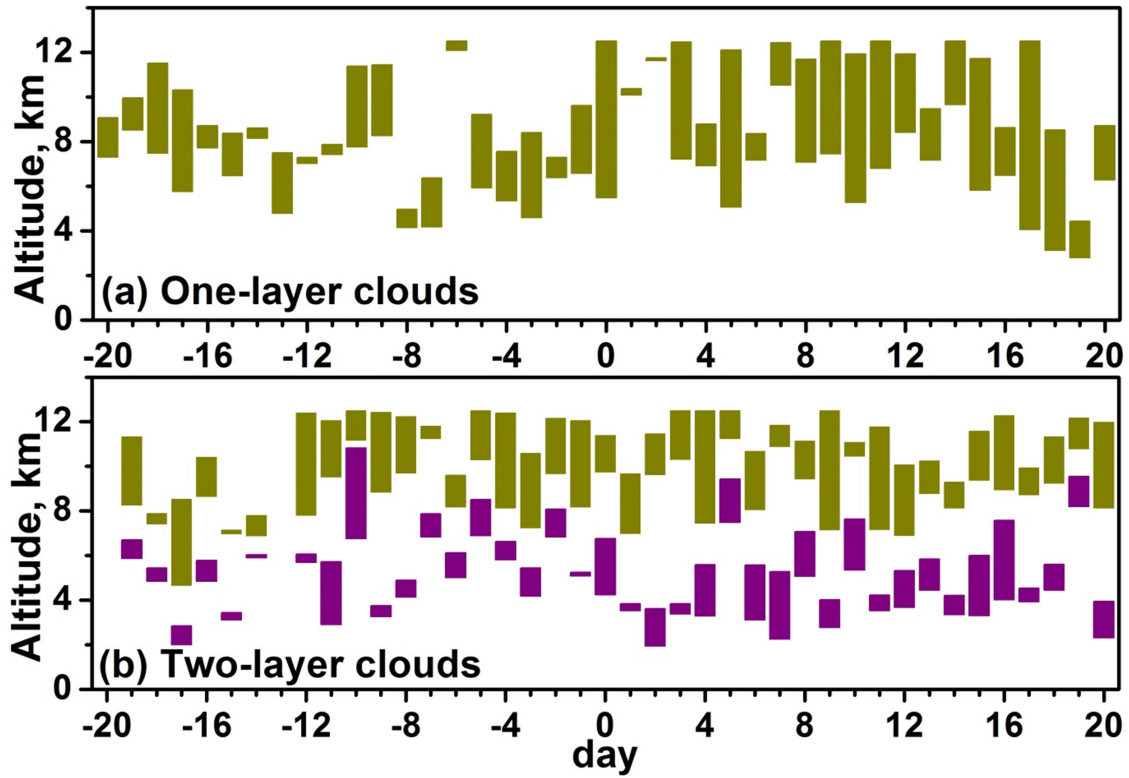
954



955

956 **Figure 12.** Composite (2006-2016) percentage occurrence of (a) clear and cloud conditions,
 957 (b) low-level, middle-level, high-level and deep convective cloud, and (c) one-, two-, three-
 958 and four or more- layer clouds observed with respect to the date of monsoon arrival over
 959 Gadanki location. Zero in x-axis indicates the date of monsoon arrival over Gadanki
 960 location.

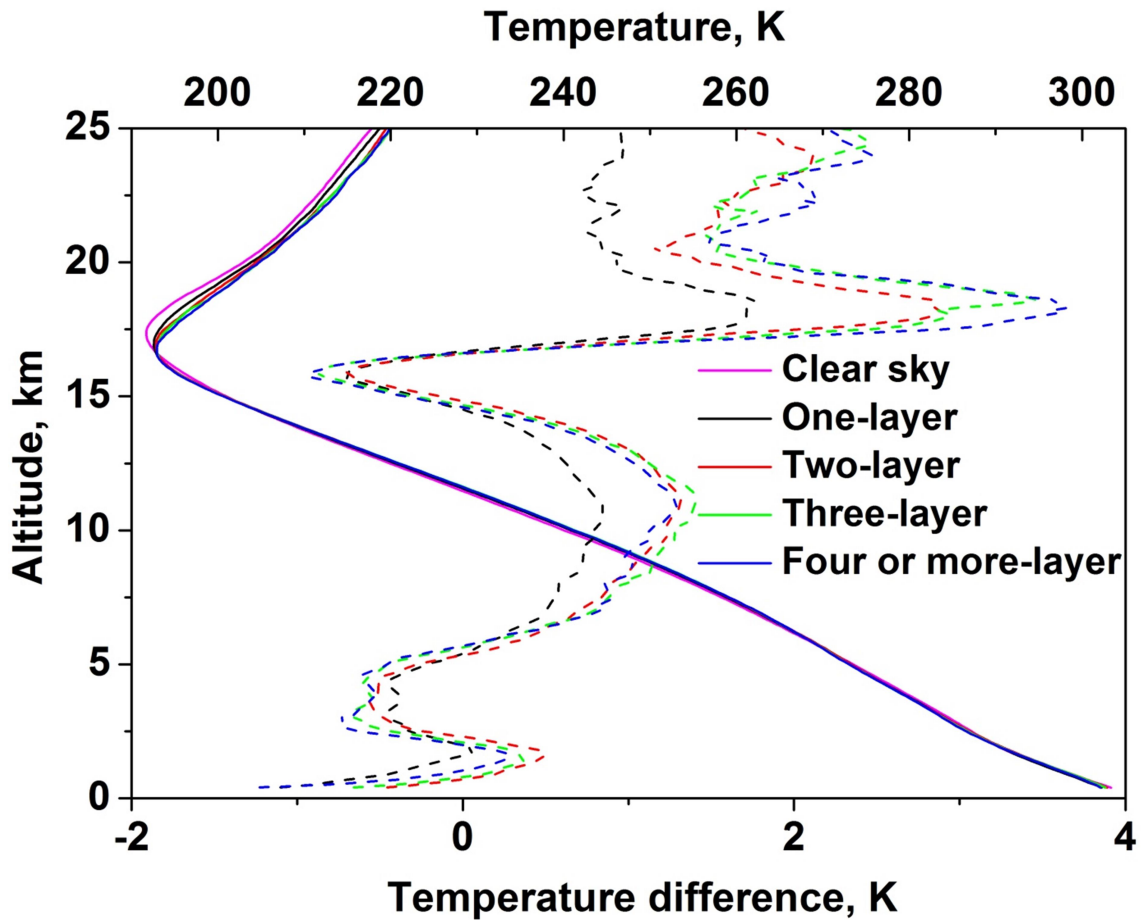
961



962

963 **Figure 13.** Composite (2006-2016) variations of mean vertical locations (base and top),
 964 thicknesses of one-layer clouds and two-layer clouds observed with respect to the date of
 965 monsoon arrival over Gadanki location. Zero in x-axis indicates the date of monsoon arrival
 966 over Gadanki location.

967



968

969 **Figure 14.** Composite (2006 – 2016) temperature profiles during clear sky, one-layer, two-
 970 layer, three-layer and four or more-layer cloud occurrences. The respective temperature
 971 difference profiles from clear sky conditions are shown with dash lines.

972

973

974

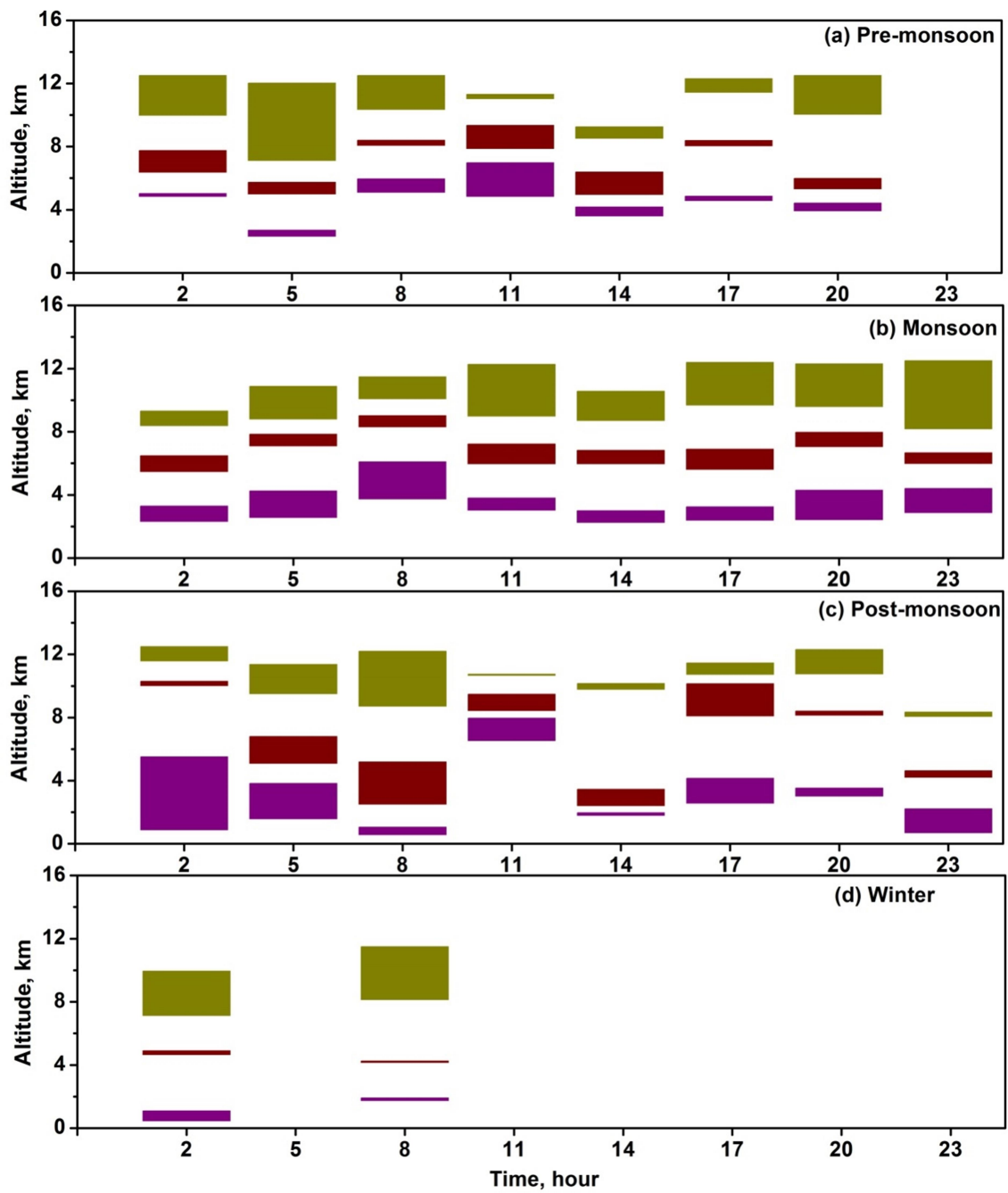
975

976

977

978

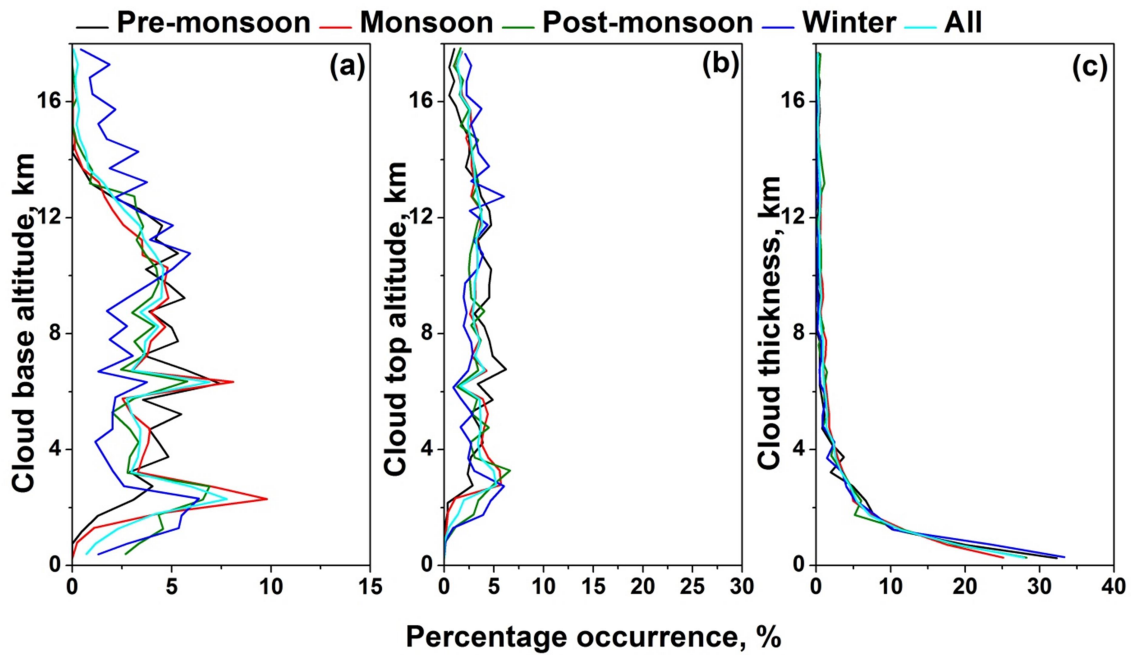
979



981

982 **Figure S1.** Diurnal variations of mean vertical locations (base and top), thicknesses of three-
 983 layer clouds observed during (a) pre-monsoon, (b) monsoon, (c) post-monsoon, and (d)
 984 winter seasons.

985



986

987 **Figure S2.** Percentage occurrence of the (a) cloud base altitude, (b) cloud top altitude and (c)

988 cloud thickness observed during different seasons over Gadanki. Altitude bin size is 500 m.